CHEMISTRY OF MATERIALS
Cite This: Chem. Mater. 2019, 31, 3929−3940
Article
pubs.acs.org/cm

Dual Strategic Approach to Prepare Defluorinated Triazole-Embedded Covalent Triazine Frameworks with High Gas Uptake Performance

Soumya Mukherjee,[†,‡] Monojit Das,[†,‡] Anupam Manna,[†,‡] Rajamani Krishna,[§] and Sanjib Das*,[†,‡]

[†]Department of Colloids & Materials Chemistry, CSIR-Institute of Minerals & Materials Technology, Bhubaneswar 751013, India
[‡]Academy of Scientific and Innovative Research (AcSIR), Ghaziabad 201002, India
[§]Van't Hoff Institute for Molecular Sciences, University of Amsterdam, Science Park 904, Amsterdam 1098 XH, The Netherlands

Supporting Information

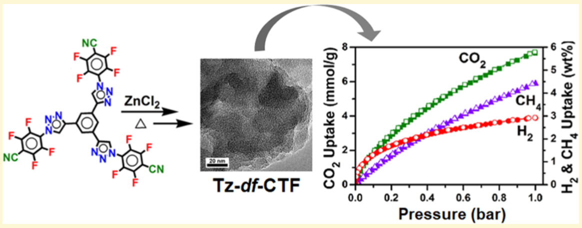

ABSTRACT: A dual strategic approach has been adopted via judicious design and synthesis of a new triazole-substituted perfluorinated aromatic nitrile (Tz-PFCN) building block to prepare three defluorinated triazole-embedded covalent triazine frameworks (Tz-*df*-CTFs) via $ZnCl_2$-catalyzed ionothermal process for high-capacity capture of small gases, especially CO_2, H_2, and CH_4. Our approach combines the incorporation of both thermally sacrificial fluorine functionality as the origin of abundant microporosity and multi-N-containing triazole functionality as strong CO_2-philic unit into the building block, which integrates high surface area (up to 2106 $m^2\ g^{-1}$) and pore volume (up to 1.43 $cm^3\ g^{-1}$) largely dominated (>90%) by narrow- and ultra-micropores together with high nitrogen and oxygen heteroatom content in the resulted Tz-*df*-CTF materials. The high microporosity in Tz-*df*-CTFs is mainly generated through the in situ defluorination process of the perfluorinated Tz-PFCN building block during the ionothermal process, and pore surfaces embedded with CO_2-philic basic N-active sites as both triazole and triazine moieties confer the frameworks with the highest amount of CO_2 capture (7.65 mmol g^{-1} at 273 K, 1 bar) and H_2 storage (2.91 wt % at 77 K, 1 bar) capability among all known porous organic polymers, including CTF systems, till date. The methane uptake capacity (4.41 wt % at 273 K, 1 bar) of these materials ranks second highest as well. A breakthrough simulation shows good separation of CO_2/N_2 (flue gas composition) and CO_2/CH_4 binary gas mixture in Tz-*df*-CTFs under industrial fixed-bed operational conditions. We anticipate that this unique dual approach will allow new opportunities toward designing and synthesizing of novel high-performing nanoporous sorbents for task-specific applications in the domain of clean energy and environmental fields.

INTRODUCTION

The exponential increase of the concentration of atmospheric carbon dioxide (CO_2) produced from the combustion of fossil fuels has raised extreme awareness on the overall impact in the global climate change.[1,2] As per the prediction of the International Energy Agency, the development of suitable porous solid sorbents that can efficiently adsorb and store CO_2 from point source postcombustion effluents, especially power plant-emitted flue gas, has an incredible prospective, which can mitigate the CO_2 emissions to a greater extent and, eventually, slow down the climate change and upcoming energy shortage crises.[3−6] Moreover, a sorbent with high-capacity CO_2 capture and separation capability has numerous industrial applications, such as in water-shift reactors, biogas purification, and natural gas upgradation. Till date, CO_2 scrubbing by aqueous amines is an extensively used technology for industrial CO_2 capture and separation involving an energy-intensive chemisorptive pathway as it is associated with high adsorption enthalpy ($Q > \sim40$ kJ mol^{-1}).[7] Despite the widespread use of the amine-based technology, it is still challenging as it suffers from serious disadvantages involving equipment corrosion, a high energy regeneration pathway, and an environmentally concerning costly discarding process of expired amine solution.[3,7] On the other hand, H_2 is an inexpensive alternative gaseous fuel abundantly available from the almost inexhaustible source of water and containing significantly higher energy density per unit mass compared with conventional fossil fuels, like petroleum and coal.[8] However, commercialization of H_2 as a practicable fuel is highly restricted by technological obstacles associated with the lack of effective and reversible viable H_2 storage systems, which spurred tremendous attention to store hydrogen in porous solid materials as an alternative energy source to substitute the current carbon-based energy resources.[9]

Most existing porous materials, like zeolites,[10,11] metal−organic frameworks,[12−14] activated carbons,[15−18] and porous organic polymers (POPs),[19−29] have been demonstrated as promising and competent candidates for high-performance gas

Received: December 31, 2018
Revised: May 16, 2019
Published: May 22, 2019

DOI: 10.1021/acs.chemmater.8b05365

storage and separation owing to their fast sorption kinetics influenced by a highly reversible energy-efficient (Q_{st} > ~40 kJ mol^{-1}) physisorptive pathway where weak van der Waals forces are associated between pore walls of the adsorbent and gas molecules, which render the sorption process with a low-energy penalty and sustainability.[30] Amongst various porous solid sorbents, POPs hold the greatest potential as emerging materials in gas adsorption and separation applications,[31−42] including catalysis,[43,44] water purification,[45,46] energy storage,[47,48] and chemo-biosensing,[49,50] owing to their enhanced physicochemical and thermal stability and highly tunable large surface area, pore volume, and pore size/shape along with superior topological and functional diversity originated via modularity in synthesis and immense choice of organic building units compared with the existing traditional solid adsorbents. Various approaches have been made to integrate organic building blocks with different dimensionalities (two-dimensional (2D), three-dimensional (3D)) and chemical functionalities mostly comprising heteroatoms, like N, O, and F, which target porous structures with large surface area and pore volume dominated by micropores and high heteroatom content to induce strong binding intensity between pore walls and gas molecules for enhancement of their adsorption and separation efficiency.[51−56] Mostly, porous structures preferably integrated with large basic N-sites and high microporous surface area are ideal for enhanced capture of polarizable acidic CO_2 molecules whereas higher adsorptive hydrogen storage capability is featured by porous solid materials having a high degree of ultra-micropores of size typically below 9 Å, combining high surface areas mostly derived from narrow- and ultra-micropores.[56,57] A recent study also found that a higher level of oxygen functionality is desirable for enhanced H_2 capture.[58] To date, a great deal of efforts has been made to develop porous organic polymers with enhanced CO_2 uptake capacities, paying very limited attention to increase their H_2 storage capabilities. Porous organic polymers categorized as best-performing CO_2 sorbents known in recent times mostly suffer from a moderate-to-low H_2 storage capability due to lack of a proper synthetic approach. Therefore, it still remains an enormous challenge to recognize more convenient and efficient approaches for developing unique porous organic materials that share the above-mentioned physicochemical properties in a synergistic manner, which could be applied as a high-capacity dual storage media for both CO_2 and H_2.

Bearing in mind these ideas, we report a dual strategic approach adopted through the rational design of a unique class of nitrogen-rich triazole-functionalized perfluorinated aromatic nitrile building blocks (Tz-PFCN) to prepare triazole-embedded covalent triazine framework (CTF)-based POPs as extraordinarily high-performing materials for small gas uptake and separation, specifically CO_2 and H_2. Our dual strategic approach mainly features the judicious integration of a thermally sacrificial large fluorine functionality (C−F) and strongly CO_2-philic multi-N-containing basic triazole unit into the Tz-PFCN building block to prepare a novel class of extremely microporous CTF-based adsorbents with high heteroatom loading, in particular, N/O active sites, exhibiting high affinity for both CO_2 and H_2 binding with improved molecular sieving capabilities. We hypothesized that integration of a large number of thermally labile C−F bonds into the building block would produce high surface area comprised of a higher degree of ultra-microporosity (pore size < 0.7 nm) to the resulted CTF materials through controlled etching of framework by in situ-generated reactive fluorinated species (CF_n) via defluorination during the high-temperature polymerization process. On the other hand, incorporation of the multi-N-containing triazole functional group comprising three different active nitrogen sites with varying basicity along with inherent triazine nitrogen in the pore surfaces of resulting frameworks would strongly boost the affinity for CO_2 owing to their most favorable electrostatic interactions with polar CO_2 molecules.[59] Further, CTF synthesis via the high-temperature ionothermal process inherently associated with O-doping (−C=O/−C−O) in the resulted frameworks would be further advantageous for H_2 capture process. Moreover, the present work also featured CO_2 uptake and separation under dynamic flowing mixed gases, such as CO_2/N_2 and CO_2/CH_4, mimicking the industrial flue gas treatment and natural gas upgradation process using the column breakthrough simulation methodology. With the present strategy of the building block design principle, the current work would provide an understanding on the synthesis of novel categories of high-performing solid sorbents with tailorable porous structures, which would find potential applications over a wide variety of technological benefits (Scheme 1).

Scheme 1. Schematic Illustration of the Formation of Tz-*df*-CTFs via a Dual Strategic Approach

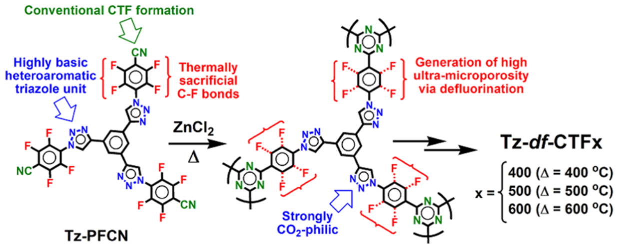

EXPERIMENTAL SECTION

Synthesis of the Building Block (Tz-PFCN). The synthesis of the building block, Tz-PFCN, was carried out by adopting the well-known Cu(I)-catalyzed "click reaction".[60] In a typical procedure, a 250 mL round bottom flask equipped with a stir bar was charged with 1,3,5-triethynylbenzene (150 mg, 0.998 mmol), 4-azidotetrafluorobenzonitrile (755 mg, 3.49 mmol), tetrahydrofuran (60 mL), and water (15 mL). The resulting clear solution was purged with argon over 30 min at room temperature followed by addition of $CuSO_4 \cdot 5H_2O$ (78.4 mg, 0.313 mmol) and sodium ascorbate (121.5 mg, 0.613 mmol). The reaction mixture was heated to 60 °C and kept stirring for 3 days under an inert atmosphere. It was filtered and evaporated to dryness followed by extraction by ethyl acetate (2 × 75 mL). The organic part was then washed with distilled water three times and dried over $MgSO_4$, followed by evaporation, resulting in a crude product, which was purified via silica gel column chromatography (ethyl acetate/petroleum ether (4:1)) to obtain a light-yellow colored compound (yield: 315 mg, 39.6%). ^1H NMR (400 MHz; DMSO-d_6): δ (ppm) 8.66 (s, 3H, Ar-H), 9.44 (s, 3H, triazole-H). ^{19}F NMR (400 MHz; DMSO-d_6): −133.58 (m, 6F), −145.62 (m, 6F). FT-IR (ATR, 400−4000 cm^{-1}): 3550, 3147, 2965, 2248, 1653, 1619, 1507, 1389, 1295, 1155, 1097, 1033, 997, 891, 827, 763.

Synthesis of Tz-*df*-CTF Materials. All Tz-*df*-CTF materials were synthesized under an ionothermal condition as described in the literature by Thomas and co-workers[61] with a slight alteration as follows. The typical experimental procedure involved transfer of triazole-functionalized perfluorinated aromatic trinitrile (Tz-PFCN) building blocks (500 mg) and anhydrous $ZnCl_2$ salt (854 mg) with a molar ratio of 1:10 into a quartz ampoule under an inert atmosphere.

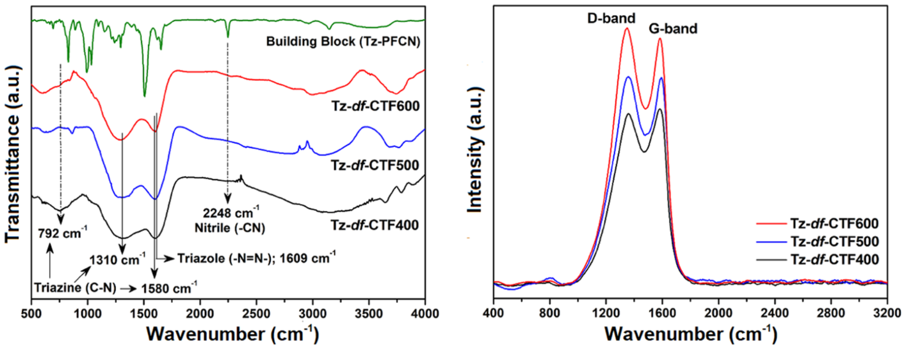

Figure 1. FT-IR (left) and Raman (right) spectra of Tz-PFCN ligand and Tz-*df*-CTFs.

The ampoule was then evacuated, flame-sealed under vacuum, and slowly heated (10° min^{-1}) to the desired temperature inside a furnace. Once the desired temperature was achieved, heating was continued for another 42 h. The ampoule was cooled down to ambient temperature and opened. It is worth mentioning that the ampoule is under high pressure, which is released while opening. The resultant black solid was collected and stirred in distilled water (200 mL) for 48 h to remove the majority of the $ZnCl_2$ salt. The product was isolated via filtration and further stirred in 1 N HCl (200 mL) for 48 h to eliminate further the residual salt. The resulting solid was finally filtered and washed repeatedly with water until neutral pH was attained in the filtrate. Finally, the solid was washed with alcohol and acetone and dried under vacuum at 100 °C for 6 h, a set of light weight black powders with yield around 56% (Tz-*df*-CTF400), 50% (Tz-*df*-CTF500), and 48% (Tz-*df*-CTF600) were obtained with respect to the starting monomer (Tz-PFCN) by mass.

■ RESULTS AND DISCUSSION

Synthesis and Characterization of Tz-*df*-CTFs. The nitrogen-rich triazole-substituted aromatic perfluoro trinitrile building block, namely, Tz-PFCN, was synthesized via a copper(I)-catalyzed alkyne-azide click reaction between 1,3,5-triethynylbenzene and 4-azidotetrafluorobenzonitrile precursor, as depicted in Scheme S1.[62] Fourier transform infrared (FT-IR) and ^{1}H and ^{19}F NMR spectroscopy were used to characterize the monomeric building block (see Supporting Information). The synthesis of Tz-*df*-CTFs was carried out via Lewis acid (anhydrous $ZnCl_2$)-catalyzed trimerization of Tz-PFCN adopting ionothermal conditions, as reported by Thomas et al.[61] In a typical synthetic procedure, C3-symmetric Tz-PFCN building blocks were cyclotrimerized by direct heating in molten zinc chloride inside a flame-sealed quartz tube where $ZnCl_2$ performed as both a Lewis acid catalyst and reaction medium. We have chosen a 10:1 molar ratio of the $ZnCl_2$ to Tz-PFCN building block since the higher amount of Zn salt would take into account the solubility issue of the high-molecular weight Tz-PFCN monomer under ionothermal condition to make the polymerization process proceed in a uniform and controlled manner.[51] Moreover, a higher molar ratio of $ZnCl_2$ is desirable to induce rich textural properties mostly suitable for capturing small gases.[51] We have carried out the polymerization reactions at 400, 500, and 600 °C for 42 h using 10 equivalents of $ZnCl_2$ resulting in a black monolithic material with a moderate yield in each case. The resulting materials are abbreviated now onward as Tz-*df*-CTF*x*, where *x* denotes polymerization temperature, Tz represents the triazole functionality, and df stands for complete defluorination. Tz-*df*-CTF materials are completely insoluble in water, dilute acids, and bases as well as common organic solvents, suggesting the formation of 3D networks with excellent chemical stability.

The successful formation of Tz-*df*-CTFs was confirmed by various analytical and spectroscopic techniques, such as elemental analysis, FT-IR, Raman, X-ray photoelectron spectroscopy (XPS), and powder X-ray diffraction (PXRD). As shown in Figure 1, the disappearance of the intense characteristic C≡N stretching band at around 2248 cm^{-1} and the emergence of two new characteristic broad bands at around 1310 and 1580 cm^{-1} corresponding to the C−N stretching and breathing mode of the triazine ring indicated the formation of fully condensed triazine-based Tz-*df*-CTF materials via cyclotrimerization of nitrile groups.[55,63,64] An additional characteristic breathing mode at around 792 cm^{-1} corresponding to the triazine unit is clearly observed for the 400 °C material, whereas at higher synthesis temperature (500 and 600 °C), this vibration band is almost featureless.[39,64]

A broad IR band peaking at around 1609 cm^{-1} is assigned as the characteristic −N═N− stretching mode of 1,2,3-triazole ring, indicating the existence of triazole moiety in all Tz-*df*-CTFs, which is well in agreement with the literature.[65,66,71] Therefore, FT-IR analysis is evident for the presence of both triazine and triazole groups in Tz-*df*-CTFs and broadening of IR peaks might be attributed to the partial carbonization and decomposition associated with the materials.[51,67,68]

To get a more detailed scenario of the extent of structural degradation in as-synthesized Tz-*df*-CTFs as a function of temperature, combustion elemental analysis is performed (Table S1). The analysis reveals much lower nitrogen content and higher C/N ratio as compared with the theoretically calculated values, which slowly grows with increase in temperature, indicating a significant loss of nitrogen during polymerization because of partial structural decomposition. The decomposition process apparently proceeds mainly via C−H and [CN] elimination involving different reactive intermediates and mechanistic pathways, and it becomes prominent for CTFs prepared by utilizing a higher molar ratio (≥10) of $ZnCl_2$ salt to monomer as well as increasing polymerization temperature.[37,69−71]

The X-ray photoelectron spectroscopy is conducted to get more precise information of the network formation, purity, chemical compositions, and bonding patterns of all Tz-*df*-CTFs. The survey spectrum reveals the existence of only carbon, nitrogen, and oxygen spectroscopic signatures with nitrogen element contents of 8.9, 7.70, and 6.30 wt % and oxygen element contents of 12.4, 12.87, and 13.60 wt % for Tz-*df*-CTF400, Tz-*df*-CTF500, and Tz-*df*-CTF600, respectively (Figure S5). The appearance of the oxygen signal is plausibly due to the decomposition of the framework via different reaction pathways involving reactive benzyne-type and/or

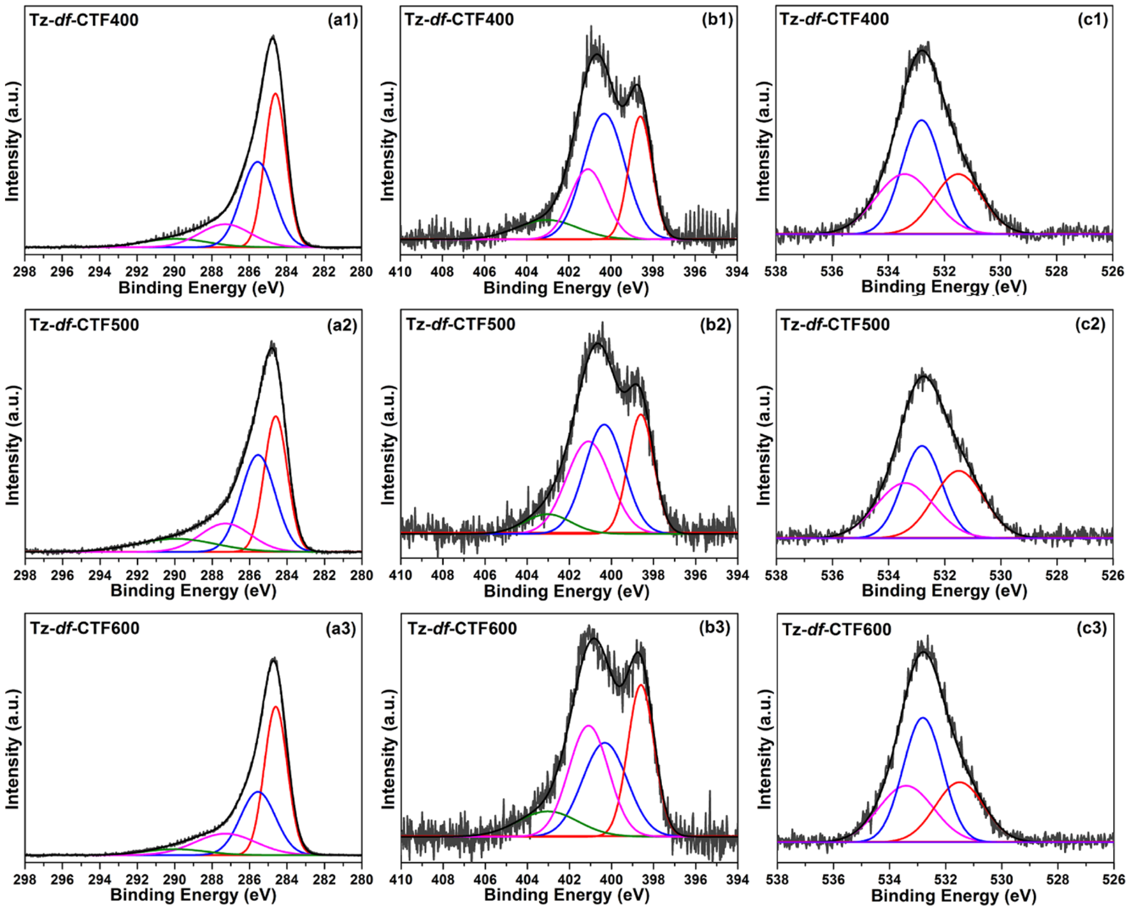

Figure 2. High-resolution XPS spectra of Tz-*df*-CTFs material: (a1−a3) C 1s, (b1−b3) N 1s, and (c1−c3) O 1s deconvoluted spectra.

radical intermediates, which can subsequently react with oxygen and/or moisture during open air aqueous workup as well as trapped atmospheric oxygen and/or moisture within the highly porous polymeric networks.[63,70,72] No residual signals for zinc species, including $ZnCl_2$, were observed in the XPS analysis. The complete removal of zinc salt during the acid−water washing process indicates the overall formation of an interconnected well-organized porous architecture. Fluorine units completely disappear in all Tz-*df*-CTFs under a high-temperature (400−600 °C) ionothermal condition, as revealed by the complete absence of any signature peak for fluorine in XPS analysis, which is well in agreement with the previous report on the thermal C−F bond cleavage in single-wall carbon nanotubes[73] and related CTF-based materials synthesized under similar conditions.[63] Moreover, a deeper understanding of the chemical bonding nature of C, N, and O atoms in Tz-*df*-CTF materials was obtained from high-resolution core-level XPS spectra of C 1s, N 1s, and O 1s (Figure 2). The deconvoluted C 1s spectra of Tz-*df*-CTFs are composed of four peaks with binding energies of 284.6, 285.55, 287.29, and 289.95 eV. The dominant signal peaking at 284.6 eV corresponds to the sp^2-hybridized double-bonded carbon atoms, whereas the peak with binding energy of 285.55 eV refers to the sp^3-hybridized carbon atoms bonded to nitrogen/oxygen atoms (C−O/C−N). The third peak with binding energy of 287.29 eV is assigned to sp^2-hybridized carbon atoms attached to nitrogen/oxygen atoms (C═N/C═O), and the weakest peak with binding energy 289.95 eV is featured in the $\pi-\pi^*$ transition.[74−76] Similarly, the N 1s spectrum of Tz-*df*-CTF materials is also deconvoluted into four distinct peaks with binding energies of 398.6, 400.32, 401.09, and 403.03 eV. The first peak centered at 398.6 eV is attributed to the hexagonal pyridinic nitrogen (−C═N) that mainly originates from the triazine unit, whereas signals located at 400.32 and 401.09 eV are associated with the single-bonded nitrogen (<u>**N**</u>−N═N) and the double-bonded nitrogen atom (N−<u>**N═N**</u>) derived from embedded triazole moiety inside all frameworks.[75,77,78] A minor amount of oxidized N species (N−O) with a binding energy of 403.03 eV is observed as well.[74,75] Thus, core-level XPS analysis further supports the existence of triazine and triazole units in all Tz-*df*-CTFs in spite of carbonization and decomposition process associated during their formation pathway, which is in accordance with the FT-IR analysis and literature. Moreover, the oxygen signal can be fitted into three peaks with binding energies of around 531.5, 532.8, and 533.4 eV. The first peak corresponds to O═C and the last peak is assigned to O−C (28.4−31.8%), both of which are consistent with the C 1s signal analysis result.[79,80] The second peak at around 532.8 eV appears due to adsorbed oxygen and/or moisture inside the Tz-*df*-CTF network.[72]

Raman spectroscopy is further employed to analyze Tz-*df*-CTF materials (Figure 1). All Tz-*df*-CTFs show two well-defined virtually superimposed Raman bands centered at around 1354 and 1585 cm^{-1} similar to the characteristic D and G Raman band, respectively, typically observed in partially graphitic amorphous carbon materials. The complete disappearance of the sharp intense Raman band (∼2252 cm^{-1}) for the cyano group further confirms the formation of fully

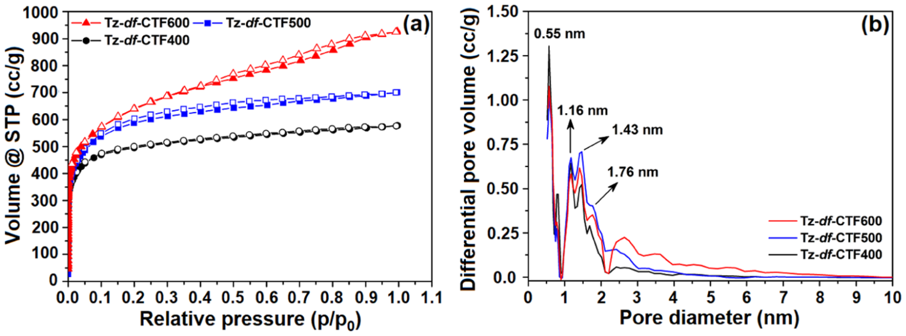

Figure 3. (a) Nitrogen adsorption−desorption isotherms of Tz-*df*-CTFs measured at 77 K (solid and open symbols represent adsorption and desorption, respectively). (b) Pore size distribution (PSD) curves of Tz-*df*-CTFs derived from the N_2 adsorption isotherm (77 K).

condensed Tz-*df*-CTF networks, as also observed from FT-IR analysis. In general, D band occurs from sp^2-hybridized carbon atoms with defects, i.e., a disordered graphite structure, whereas G band is related to the first-order scattering of the E_{2g} mode for sp^2-hybridized carbon atoms in a two-dimensional hexagonal graphitic layer structure. I_D/I_G values of 0.97, 1.01, and 1.04 for Tz-*df*-CTF400, Tz-*df*-CTF500, and Tz-*df*-CTF600, respectively, indicate the fact that with increasing polymerization temperature from 400 to 600 °C, the structural defects also increase as the extent of structural decomposition becomes higher at higher synthesis temperature, resembling the result obtained from elemental analysis of Tz-*df*-CTFs.[81−83] The CTF-based materials are mostly amorphous in nature except a few, like CTF-0, CTF-1, and CTF-2, that show moderate crystallinity.[61,84,85] As expected, the wide-angle powder X-ray diffraction analysis of Tz-*df*-CTF materials (Figure S6) showed a featureless diffraction pattern with two extremely broad peaks at around $2\theta = 24.45°$ (d_{002} = 3.64 Å) and $2\theta = 43.28°$ (d_{100} = 2.08 Å), confirming the formation of a partially graphitized amorphous polymeric structure. However, the estimated d_{002} for Tz-*df*-CTFs is larger than that of the characteristic ideal d_{002} value of 3.35 Å observed in a pure graphite layer. Thus, both Raman and PXRD analysis indicate a random combination of a small disordered graphitic layer structure induced by significant N- and O-doping into the layers.

The modality of Tz-*df*-CTFs was further analyzed by field-emission scanning electron microscopy (FE-SEM) and high-resolution transmission electron microscopy (HR-TEM). The FE-SEM images of Tz-*df*-CTFs exhibited a typical surface morphology of agglomerated tiny and irregular shaped particles homogenously distributed through the polymeric matrix (Figure S7). The microstructure of Tz-*df*-CTFs was observed via HR-TEM images constituting well-distributed uniform interconnected micro-and ultra-micropores (Figure S8) with a continuous polymeric phase, as indicated by the presence of homogenously distributed dark and bright areas.

Gas Adsorption Properties. The porosity parameters of Tz-*df*-CTF materials were derived using the N_2 adsorption−desorption isotherm measured at 77 K. According to the IUPAC classification, the isotherms of Tz-*df*-CTF materials can be broadly classified as type-I isotherm with some type-II character, as depicted in Figure 3a. The fully reversible isotherms of Tz-*df*-CTFs feature a steep rise in nitrogen uptake at a low relative pressure ($P/P_0 < 0.01$), which is characteristic for the existence of abundant micropores. At higher relative pressure (<0.1), a continuous steady rise of adsorption isotherms is observed for Tz-*df*-CTF600, reflecting the presence of well-developed narrow mesopores, which is most desirable for effective diffusion of incoming gas molecules into the porous networks and thereby enhancing the gas uptake capacity.[86,87] The rate of rise of the adsorption isotherm became slower for materials with a decreasing synthesis temperature, revealing lowering of the narrow mesoporosity in Tz-*df*-CTF500 and Tz-*df*-CTF400 compared with Tz-*df*-CTF600. Thus, simply by changing the synthesis temperature, fine modulation of porosity in Tz-*df*-CTF materials can be achieved. A small degree of hysteresis in the partial pressure range of 0.1−0.9 and 0.4−0.9 was observed for Tz-*df*-CTF500 and Tz-*df*-CTF400, respectively, further attributing the presence of well-organized mesopores as mostly narrow slitlike in nature. Tz-*df*-CTF400 possesses almost a flat adsorption plateau without any hysteresis between the adsorption−desorption step, indicating its exclusive microporous in nature.[88]

The specific Brunauer−Emmett−Teller (BET) surface area was estimated to be 1550 $m^2\ g^{-1}$ for Tz-*df*-CTF400, 1878 $m^2\ g^{-1}$ for Tz-*df*-CTF500, and 2105 $m^2\ g^{-1}$ for Tz-*df*-CTF600, whereas the corresponding Langmuir surface area was found to be 2068, 2388, and 2548 $m^2\ g^{-1}$ combining a total pore volume of 0.89, 1.08, and 1.43 $cm^3\ g^{-1}$, respectively. The obtained textural parameters are comparable and/or higher than those of other previously reported high-performing POP, including CTF-based materials, in the literature.[32,53,54,89−91]

The pore size distribution (PSD) was estimated by fitting the N_2 isotherm (77 K, 1 bar) with nonlocal density functional theory (NL-DFT) using a “carbon-based slit-pore” model (Figure 3b), which clearly indicates the dominance of the larger fraction of ultra-micropores with a pore diameter around 0.55 nm along with a relatively smaller fraction of narrow micropores with pore diameters of around 1.16, 1.43, and 1.76 nm. Besides, a small proportion of narrow mesopores spreading over 2−5 nm is observed as well in all Tz-*df*-CTFs. The degree of narrow mesoporosity slowly grows on increasing the synthesis temperature and becomes the highest for Tz-*df*-CTF600, making it ideal for an enhanced gas adsorption capability because the presence of narrow mesopores along with abundant micropores is greatly advantageous for the sorption process as it provides a smooth gateway for diffusion of gas molecules, whereas micropores are the most desired environment for trapping of small gas molecules.[86,87,92] The microporous surface areas and pore volumes were calculated to be 1453, 1746, and 1754 $m^2\ g^{-1}$ for Tz-*df*-CTF400, Tz-*df*-CTF500, and Tz-*df*-CTF600, respectively, whereas the corresponding micropore volumes were determined as 0.75, 0.89, and 0.91 $cm^3\ g^{-1}$ (Table 1). Since narrow

Table 1. Textural Parameters Derived from N_2 (77 K, 1 bar) and CO_2 (273 K, 1 bar) Isotherm

material	S_{BET}[a] ($m^2\ g^{-1}$)	S_{Lang}[b] ($m^2\ g^{-1}$)	S_{micro}[c] ($m^2\ g^{-1}$)	V_{micro}[d] ($cm^3\ g^{-1}$)	V_{total}[e] ($cm^3\ g^{-1}$)	$V_{(CO_2)}$[f] ($cm^3\ g^{-1}$)	N (%)[g]
Tz-*df*-CTF400	1550	2068	1453	0.75	0.89	0.088	9.63 (8.90)
Tz-*df*-CTF500	1878	2389	1746	0.89	1.08	0.095	7.97 (7.70)
Tz-*df*-CTF600	2106	2549	1754	0.91	1.43	0.099	6.15 (6.30)

[a] Calculated BET surface area from N_2 isotherm over the conventional pressure range of 0.05−0.3 bar. [b] Langmuir surface area estimated by applying the Langmuir equation on the nitrogen isotherm over the pressure range 0−0.15 bar. [c] Micropore surface area calculated using the classical *t*-plot method. [d] Micropore volume calculated at $P/P_0 = 0.1$ for pores ≤ 1.6 nm. [e] Total pore volume calculated from the N_2 isotherm based on the slit pore NLDFT equilibrium model. [f] Total pore volume (pores diameter < 1 nm) calculated from CO_2 isotherm at 273 K on the basis of the CO_2 NLDFT model at $P/P_0 = 0.15$. [g] Nitrogen content is estimated via combustion process, and values in parenthesis are determined through XPS analysis.

Table 2. Low-Pressure CO_2, CH_4, N_2, and H_2 Uptake Behavior, Heat of Adsorption, and CO_2 Selectivity over N_2 and CH_4 of the Presented Tz-*df*-CTFs

	CO_2 uptake[a]			CH_4 uptake[a]			N_2 uptake[a]		H_2 uptake[c]	selectivity[d]	
material	273 K	298 K	Q_{st}[b]	273 K	298 K	Q_{st}[b]	273 K	298 K	77 K	CO_2/N_2	CO_2/CH_4
Tz-*df*-CTF400	6.42 (2.32)	4.32 (1.33)	23.4	2.27	1.08	27.4	1.04	0.46	2.51	18.5 (22.7)	7.5 (8.0)
Tz-*df*-CTF500	7.41 (2.36)	4.86 (1.35)	19.7	2.58	1.34	22.5	1.29	0.50	2.76	18.9 (21.5)	6.2 (7.2)
Tz-*df*-CTF600	7.65 (2.39)	5.08 (1.36)	20.0	2.76	1.32	24.0	1.32	0.53	2.91	16.8 (21.1)	5.8 (5.7)

[a] Gas uptake in mmol g^{-1} at 1 bar and values in parenthesis in mmol g^{-1} at 0.15 bar. [b] Isosteric heat of adsorption in kJ mol^{-1}. [c] Gas uptake in wt % at 1 bar. [d] Calculated by ideal adsorbed solution theory (IAST) method at a molar ratio of 15:85 for CO_2/N_2 and 50:50 for CO_2/CH_4 whereas values in parenthesis are calculated from the ratio of the initial slopes in the Henry region of the respective CO_2, CH_4, and N_2 adsorption isotherms at 298 K.

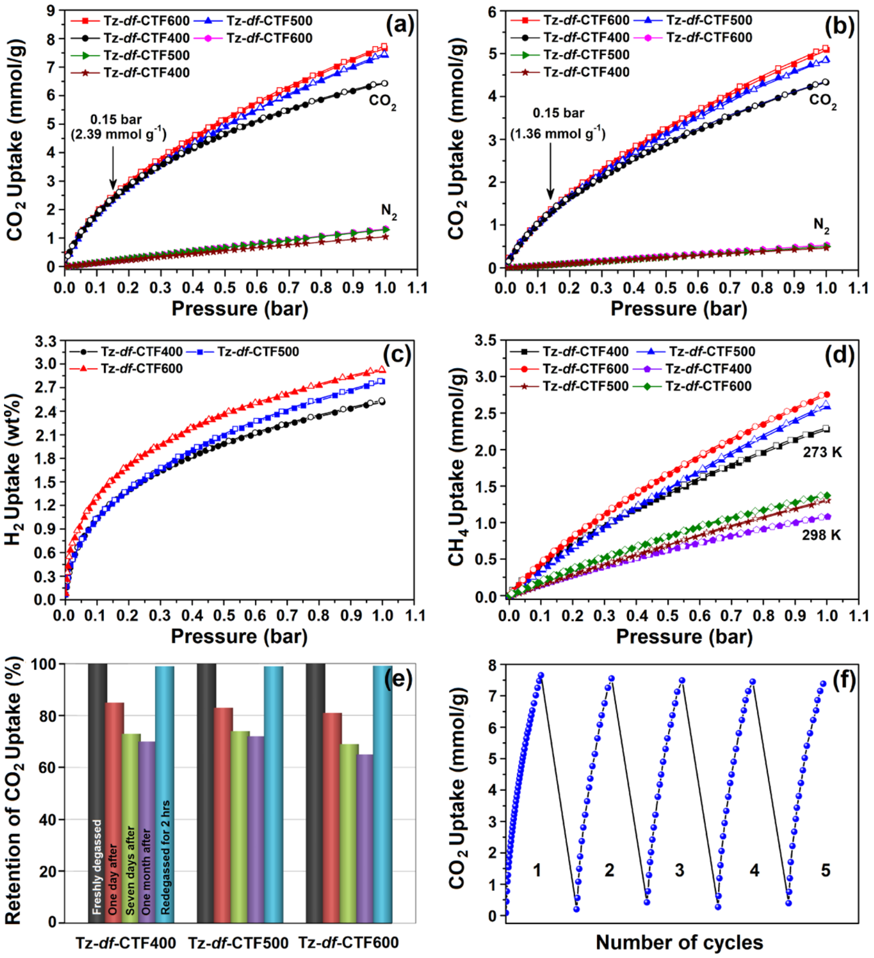

Figure 4. CO_2 and N_2 isotherms measured at (a) 273 K and (b) 298 K. (c) H_2 isotherms measured at 77 K. (d) CH_4 isotherms measured at 273 and 298 K. (e) CO_2 uptake (298 K, 1 bar) with humidified samples. (f) Reusability test for five cycles of CO_2 uptake (273 K, 1 bar) of Tz-*df*-CTF600. Filled and open symbols represent adsorption and desorption, respectively.

DOI: 10.1021/acs.chemmater.8b05365
Chem. Mater. 2019, 31, 3929−3940

microporosity is one of the most desirable parameters for enhanced gas uptake capacity in porous materials, we have further used CO_2 adsorption isotherm (273 K, 1 bar) to derive better resolved PSD by nonlocal density functional theory (NL-DFT) utilizing a carbon-based slit-pore model to have more details and precise microporous (0.3−1.0 nm) structural information of Tz-*df*-CTFs (Figure S9).[93] A careful examination of PSD curves shows that the dominance of ultra-micropores (<7 Å) in Tz-*df*-CTFs slowly increases with increasing synthesis temperature along with the increase of CO_2 accessible micropore volume $V_{\text{micro}}(CO_2)$ from 0.088 to 0.099 $cm^3\ g^{-1}$. The large pore volume and significantly high surface area dominated by extremely large fractions of narrow- and ultra-micropores was mainly originated via $ZnCl_2$-assisted defluorination process during the high-temperature polymerization reaction where thermally sacrificial aromatic C−F bonds undergo a complete defluorination process resulting in situ generation of extremely reactive fluorinated species (CF_n), which subsequently etch the polymeric backbone while releasing out from the polymeric matrix, thus creating fine defects on the polymer backbone.

The abundant narrow- and ultra-micropore, high N,O-heteroatom content, including impressive physicochemical and thermal stability, inspired us to investigate their gas uptake capabilities, especially CO_2, H_2, and CH_4, relevant to environment and energy applications, which is summarized in Table 2. First, the CO_2 uptake capacity was assessed by CO_2 isotherms measured at T = 273 and 298 K up to 1 bar. As shown in Figure 4, all Tz-*df*-CTFs adsorb exceptionally high CO_2 with an uptake capacity of 6.42 mmol g^{-1} (Tz-*df*-CTF400), 7.41 mmol g^{-1} (Tz-*df*-CTF500), and 7.65 mmol g^{-1} (Tz-*df*-CTF600) at 273 K and 1.0 bar. Similarly, at 298 K and 1.0 bar, they exhibit extremely high CO_2 adsorption as well as uptake values of 4.32 mmol g^{-1} (Tz-*df*-CTF400), 4.86 mmol g^{-1} (Tz-*df*-CTF500), and 5.08 mmol g^{-1} (Tz-*df*-CTF600). To the best of our knowledge, the obtained CO_2 adsorption values of both Tz-*df*-CTF500 and Tz-*df*-CTF600 represent the highest CO_2 uptake capacity so far among all known POPs, including CTF-based materials (Tables S6 and S7).[32,36,55,56,89,94−96] The exceptionally high CO_2 philicity of Tz-*df*-CTFs can be correlated mainly by two major desirable parameters, such as (i) large surface area that arises almost entirely from narrow- and ultra-micropores, which is most suitable for trapping both polar (CO_2) and nonpolar (H_2 and CH_4) gas molecules and (ii) significantly high basic N sites derived from embedded highly polar functionalities like triazine and triazole moieties with strong affinity for polar and acidic gas molecules like CO_2, which synergistically contribute to the exceptionally high CO_2 uptake ability. However, it is worth mentioning that Tz-*df*-CTF600 with slightly lower N content shows the highest CO_2 uptake compared with Tz-*df*-CTF500 and Tz-*df*-CTF400, which clearly indicates that nitrogen content alone weakly influences the CO_2 uptake capacity. Therefore, CO_2-accessible micropore volume and high surface area combining extensive microporosity are the more decisive factors in combination with N content for the observed high CO_2 uptake in the newly introduced Tz-*df*-CTF materials.

The H_2 storage capability of Tz-*df*-CTFs was investigated at 77 K and 1 bar since hydrogen storage at cryogenic temperature under ambient pressure condition has recently gained enormous attention as being viable for low-pressure vehicular hydrogen storage for safe transportation.[97] Figure 4c shows that Tz-*df*-CTF400, Tz-*df*-CTF500 and Tz-*df*-CTF600 exhibit unprecedentedly high H_2 uptakes of 2.51, 2.76, and 2.91 wt %, respectively. To date, Tz-*df*-CTF600 with a H_2 uptake capacity of 2.91 wt % superseded all reported best performing POP and CTF-based adsorbents (Tables S6 and S7).[53,56,89,96,98,99] It is worth mentioning that Tz-*df*-CTFs demonstrate excellent reproducibility toward H_2 uptake and retention of more than 98% of H_2 uptake capability even after five repeated cycles of uptake in experiment. Tz-*df*-CTFs show impressive CH_4 adsorption at 273 K and 1 bar (Figure 4d) with an uptake capacity of 2.27 mmol g^{-1} (3.63 wt %), 2.58 mmol g^{-1} (4.12 wt %), and 2.76 mmol g^{-1} (4.41 wt %), representing the second highest value among known POPs and related CTFs with the only exception of the recently reported TPC-1 material (Table S8).[63] The CH_4 uptake capacities of these materials are high as well at 298 K and 1 bar, with the maximum uptake of 1.32 mmol g^{-1} (2.20 wt %) for Tz-*df*-CTF600. The high surface area mostly derived from narrow- and ultra-micropores combining large pore volume is the most plausible parameter responsible for high uptake of nonpolar gases, like H_2 and CH_4. A comparative analysis of porosity parameters and gas uptake (CO_2, H_2, and CH_4) capacities of Tz-*df*-CTFs with the current benchmark porous organic polymers, including CTFs, is summarized in Table S9.

To get a qualitative understanding of the interaction between Tz-*df*-CTF materials and gas molecules, isosteric heat of adsorption (Q_{st}) was calculated employing the Clausius−Clapeyron equation from the adsorption isotherms measured at T = 273 and 298 K (see Supporting Information). For CO_2 adsorption, Tz-*df*-CTFs exhibit fairly good Q_{st} values in the range 19.7−23.4 kJ mol^{-1} and remain almost constant as a function of CO_2 loading, indicating the existence of strong interaction between Tz-*df*-CTF skeleton and CO_2 molecules. Likewise, Q_{st} values for CH_4 adsorption are estimated in the range 22.5−27.4 kJ mol^{-1} for all Tz-*df*-CTFs.

To better highlight the practical efficiency of our Tz-*df*-CTF materials as a CO_2 adsorbent for more realistic postcombustion applications such as flue gas (CO_2 content is only ∼15% at a total pressure of 1 bar) treatment, the high CO_2 uptake capability at 0.15 bar (∼CO_2 partial pressure in flue gas) is a highly desired feature. As shown in Table 2, all Tz-*df*-CTFs exhibit more than 2.30 mmol g^{-1} (maximum up to 2.39 mmol g^{-1}) CO_2 uptake at 0.15 bar, which represents the highest value among known POP and CTF-based materials except for very recently reported HAT-CTFs (3.0 mmol g^{-1}).[32,35,55,98,100,101] High CO_2 uptake capability in the low-pressure (0.15 bar) region further lead us to evaluate the selectivity of CO_2 over N_2 in a CO_2/N_2 (15:85) binary mixture comprising of equilibrium partial pressure of 0.85 bar (N_2) and 0.15 bar (CO_2) in the bulk phase using the well-known ideal adsorbed solution theory (IAST) model at ambient condition (see Supporting Information for details).[102] Moreover, the selectivity of CO_2 over CH_4 (50:50) was also calculated at an equilibrium partial pressure of 0.50 bar for CO_2 and 0.50 bar for CH_4 in the bulk phase, mimicking the natural gas upgradation process.[103,104] Tz-*df*-CTFs demonstrate almost similar CO_2-over-N_2 selectivity of 16.8−18.9, whereas the range is 5.8−7.6 for CO_2-over-CH_4. The similar selectivity values among Tz-*df*-CTFs may be ascribed to the little difference in their CO_2 uptake capabilities and almost identical porous architecture in the narrow- and ultra-microporous region. For the sake of comparison, the Henry selectivity values

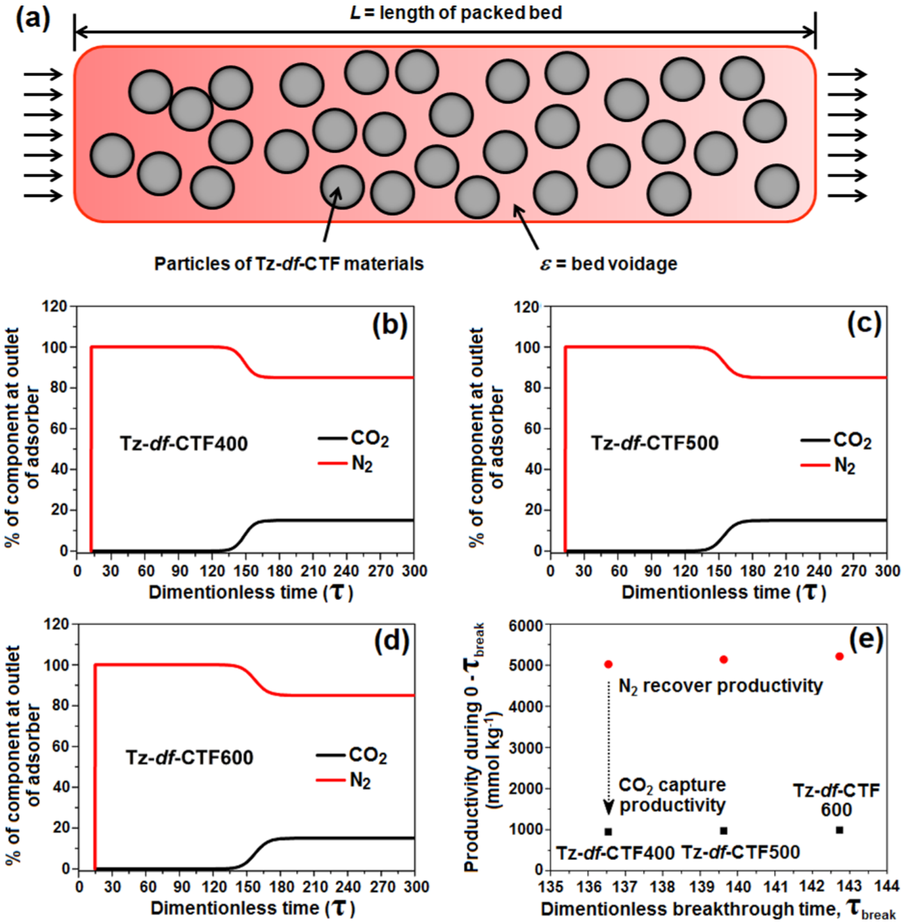

Figure 5. (a) Schematic of a packed bed adsorber for Tz-*df*-CTFs. (b−d) Breakthrough characteristic in the separation of 15% CO_2 + 85% N_2 binary mixture at 298 K. (e) Comparison of CO_2 capture and N_2 recovery productivity at 298 K.

for CO_2/N_2 and CO_2/CH_4 were calculated to be in the range 22.7−21.1 and 5.7−8.0, respectively, at ambient condition.

The unprecedented CO_2 uptake capabilities of Tz-*df*-CTFs encouraged us to test the potential of applying them in more realistic applications where moisture stability is a critical requirement. In this context, Tz-*df*-CTFs were stored under open atmospheric conditions (humidity range: 60−65%) for a month whereas CO_2 uptake capacities were measured at a different time interval during the specified time period. As shown in Figure 4e, Tz-*df*-CTF500 retained almost 72% of the total CO_2 uptake capacity whereas Tz-*df*-CTF600 exhibited 65% retention of CO_2 uptake capacity even after 30 days. The original CO_2 uptake capacity of all frameworks was restored to its original position after re-degassing the samples at 140 °C for 2 h under dynamic vacuum condition.

Transient Breakthrough Simulations. As described earlier by Krishna and Long group, the transient breakthrough simulations were conducted to validate the feasibility of utilizing Tz-*df*-CTF materials to reflect the separation ability of binary 15:85 CO_2/N_2 and 50:50 CO_2/CH_4 gas mixtures of a pressure swing adsorption process for industrial-scale capture (see Supporting Information for details).[105−109] Figure 5a shows a schematic representation of a typical packed-bed column as a model of an industrial fixed bed adsorber. Figure 5b−d represents typical breakthrough curves for the separation of 15:85 CO_2/N_2 and 50:50 CO_2/CH_4 binary gas mixtures in Tz-*df*-CTFs. Complete separations of 15:85 CO_2/N_2 and 50:50 CO_2/CH_4 were realized with all Tz-*df*-CTFs whereby N_2 and CH_4 breakthrough occurred first almost immediately through the bed and then CO_2 eluted through the fixed bed after a certain time, τ_{break}. During a certain time interval, 0−τ_{break}, nearly pure N_2 or CH_4 can be recovered from the gas mixture exiting the adsorber. For a quantitative estimation, we arbitrarily set the outlet gas purity requirement for N_2 and CH_4 as 99% in the separation process and calculated the productivity during time interval of 0−τ_{break}. On the basis of the mass balance on the packed bed adsorber, the productivity of pure N_2 with 99% purity exiting the adsorber was 5019.15, 5134.10, and 5210.72 mmol kg^{-1} and the corresponding amount of captured CO_2 on the adsorber was 942.52, 967.43 and 986.59 mmol kg^{-1} from the 15:85 CO_2/N_2 binary mixtures for Tz-*df*-CTF400, Tz-*df*-CTF500, and Tz-*df*-CTF600, respectively, which are comparable to known related materials.[109,110] Similarly, the productivity of 99% pure CH_4 at the outlet of the adsorber during the 0−τ_{break} time interval was 2030.65, 2136.01, and 2097.70 mmol kg^{-1} whereas the amount of captured CO_2 on the adsorber reached 2605.36, 2605.36, and 2385.05 mmol kg^{-1} from the 50:50 CO_2/CH_4 binary mixture for Tz-*df*-CTF400, Tz-*df*-CTF500, and Tz-*df*-CTF600 material, respectively.

■ CONCLUSIONS

To conclude, we have introduced a dual strategic approach via judicious design and synthesis of perfluorinated nitrogen-rich triazole-functionalized trinitrile building blocks to prepare highly N/O-doped extremely microporous CTF-based POPs

(Tz-*df*-CTFs) adopting conventional ionothermal synthesis and investigated their applicability as high-performance CO_2, CH_4, and H_2 adsorbents. The Tz-*df*-CTF materials feature large surface areas (up to 2106 m^2 g^{-1}) mostly attributed (up to 93%) to extremely narrow- and ultra-micropores and high N/O heteroatom content, which synergistically endow Tz-*df*-CTFs with exceptionally large CO_2 uptake capability up to 7.65 mmol g^{-1} (273 K, 1 bar) and 5.08 mmol g^{-1} (298 K, 1 bar) and H_2 storage capability up to 2.91 wt % (77 K, 1 bar). Both CO_2 and H_2 uptake values of Tz-*df*-CTFs set a new benchmark among all known POPs. Moreover, the excellent cycling ability makes them potential materials to be reused. Our dual strategic approach reveals a unique guideline on the benefit of using building blocks comprising extensive content of both CO_2-philic multi-N-containing heterocyclic triazole moieties and thermally sacrificial abundant fluorine functionalities to make ideal high-performing gas sorbents based on porous organic polymers. This current approach will render some general guideline to facilitate the rational design and implementation of advanced porous materials as storage media for multitask-specific carbon capture and energy storage applications. An extended, in-depth investigation in this direction is currently ongoing by our research group.

■ ASSOCIATED CONTENT

Ⓢ Supporting Information

The Supporting Information is available free of charge on the ACS Publications website at DOI: 10.1021/acs.chemmater.8b05365.

> Synthetic routes and experimental procedures of Tz-PFCN building blocks and their characterization using FT-IR and NMR spectroscopy; powder XRD, CHN analysis, FE-SEM and HR-TEM images, survey scan of XPS, and CO_2-isotherm-derived pore size distribution of Tz-*df*-CTFs; selectivity calculation using Henry's law method and ideal adsorption solution theory, column breakthrough simulation for CO_2/N_2 and CO_2/CH_4 gas mixtures under kinetic flow condition and productivity for the CO_2/CH_4 gas mixture, comparison tables of gas uptake and textural properties (PDF)

■ AUTHOR INFORMATION

Corresponding Author

*E-mail: sanjibdas@immt.res.in. Tel: +91-674-237-9156 (O), +91-8018256830 (M). Fax: +91-674-256-7160.

ORCID

Rajamani Krishna: 0000-0002-4784-8530
Sanjib Das: 0000-0001-9223-8021

Funding

Financial and infrastructural support from The Director, Institute of Minerals & Materials Technology (IMMT) under Council of Scientific & Industrial Research (CSIR) and Science and Engineering Research Board (SERB), Govt. of India under Award No. YSS/2015/001772.

Notes

The authors declare no competing financial interest.

■ ACKNOWLEDGMENTS

S.M. acknowledges SERB, New Delhi, M.D. acknowledges UGC, and A.M. acknowledges CSIR for their research fellowship.

■ REFERENCES

(1) Intergovernmental Panel on Climate Change. *Climate Change 2014: Mitigation of Climate Change. Contribution of Working Group III to the Fifth Assessment Report of the Intergovernmental Panel on Climate Change*; Cambridge University Press: Cambridge, United Kingdom and New York, NY, 2014.

(2) International Energy Agency. *World Energy Outlook 2017*; OECD Publishing, Paris/International Energy Agency: Paris, 2017.

(3) Haszeldine, R. S. Carbon Capture and Storage: How Green Can Black Be? *Science* **2009**, *325*, 1647−1652.

(4) *Energy Technology Perspectives*; International Energy Agency: Paris, 2017.

(5) Franklin, M. O., Jr. CO_2 Capture and Storage: Are We Ready? *Energy Environ. Sci.* **2009**, *2*, 449−458.

(6) D'Alessandro, D. M.; Smit, B.; Long, J. R. Carbon Dioxide Capture: Prospects for New Materials. *Angew. Chem., Int. Ed.* **2010**, *49*, 6058−6082.

(7) Rochelle, G. T. Amine Scrubbing for CO_2 Capture. *Science* **2009**, *325*, 1652−1654.

(8) Suh, M. P.; Park, H. J.; Prasad, T. K.; Lin, D.-W. Hydrogen Storage in Metal-Organic Frameworks. *Chem. Rev.* **2012**, *112*, 782−835.

(9) Van den Berg, A. W. C.; Areán, C. O. Materials for Hydrogen Storage: Current Research Trends and Perspectives. *Chem. Commun.* **2008**, 668−681.

(10) Deng, H.; Yi, H.; Tang, X.; Yu, Q.; Ning, P.; Yang, L. Adsorption Equilibrium for Sulfur Dioxide, Nitric Oxide, Carbon Dioxide, Nitrogen on 13X and 5A Zeolites. *Chem. Eng. J.* **2012**, *188*, 77−85.

(11) Zhang, J.; Singh, R.; Webley, P. A. Alkali and Alkaline-Earth Cation Exchanged Chabazite Zeolites for Adsorption Based CO_2 Capture. *Microporous Mesoporous Mater.* **2008**, *111*, 478−487.

(12) Sumida, K.; Rogow, D. L.; Mason, J. A.; McDonald, T. M.; Bloch, E. D.; Herm, Z. R.; Bae, T. H.; Long, J. R. Carbon Dioxide Capture in Metal-Organic Frameworks. *Chem. Rev.* **2012**, *112*, 724−781.

(13) Li, J.-R.; Ma, Y.; McCarthy, M. C.; Sculley, J.; Yu, J.; Jeong, H.-K.; Balbuena, P. B.; Zhou, H.-C. Carbon Dioxide Capture-Related Gas Adsorption and Separation in Metal-Organic Frameworks. *Coord. Chem. Rev.* **2011**, *255*, 1791−1823.

(14) Liu, Y.; Wang, Z. U.; Zhou, H.-C. Recent Advances in Carbon Dioxide Capture with Metal-Organic Frameworks. *Greenhouse Gases: Sci. Technol.* **2012**, *2*, 239−259.

(15) Sevilla, M.; Fuertes, A. B. Sustainable Porous Carbons with a Superior Performance for CO_2 Capture. *Energy Environ. Sci.* **2011**, *4*, 1765−1771.

(16) Jalilov, A. S.; Ruan, G.; Hwang, C.-C.; Schipper, D. E.; Tour, J. J.; Li, Y.; Fei, H.; Samuel, E. L. G.; Tour, J. M. Asphalt-Derived High Surface Area Activated Porous Carbons for Carbon Dioxide Capture. *ACS Appl. Mater. Interfaces* **2015**, *7*, 1376−1382.

(17) Yang, J.; Yue, L.; Hu, X.; Wang, L.; Zhao, Y.; Lin, Y.; Sun, Y.; DaCosta, H.; Guo, L. Efficient CO_2 Capture by Porous Carbons Derived from Coconut Shell. *Energy Fuels* **2017**, *31*, 4287−4293.

(18) Chen, J.; Yang, J.; Hu, G.; Hu, X.; Li, Z.; Shen, S.; Radosz, M.; Fan, M. Enhanced CO_2 Capture Capacity of Nitrogen-Doped Biomass-Derived Porous Carbons. *ACS Sustainable Chem. Eng.* **2016**, *4*, 1439−1445.

(19) McKeown, N. B.; Budd, P. M. Polymers of Intrinsic Microporosity (PIMs): Organic Materials for Membrane Separations, Heterogeneous Catalysis and Hydrogen Storage. *Chem. Soc. Rev.* **2006**, *35*, 675−683.

(20) Ding, S. Y.; Wang, W. Covalent Organic Frameworks (COFs): From Design to Applications. *Chem. Soc. Rev.* **2013**, *42*, 548−568.

(21) Lu, W.; Yuan, D.; Zhao, D.; Schilling, C. I.; Plietzsch, O.; Muller, T.; Bräse, S.; Guenther, J.; Blümel, J.; Krishna, R.; Li, Z.; Zhou, H.-C. Porous Polymer Networks: Synthesis, Porosity, and Applications in Gas Storage/Separation. *Chem. Mater.* **2010**, *22*, 5964−5972.

(22) Lu, W.; Wei, Z.; Yuan, D.; Tian, J.; Fordham, S.; Zhou, H.-C. Rational Design and Synthesis of Porous Polymer Networks: Toward High Surface Area. *Chem. Mater.* **2014**, *26*, 4589−4597.

(23) Sun, L.-B.; Li, A.-G.; Liu, X.-D.; Liu, X.-Q.; Fang, D.; Lu, W.; Yuan, D.; Zhou, H.-C. Facile Fabrication of Cost-Effective Porous Polymer Networks for Highly Selective CO_2 Capture. *J. Mater. Chem. A* **2015**, *3*, 3252−3256.

(24) Martin, R. L.; Simon, C. M.; Smit, B.; Haranczyk, M. In silico Design of Porous Polymer Networks: High-Throughput Screening for Methane Storage Materials. *J. Am. Chem. Soc.* **2014**, *136*, 5006−5022.

(25) Tan, L.; Tan, B. Hypercrosslinked Porous Polymer Materials: Design, Synthesis, and Applications. *Chem. Soc. Rev.* **2017**, *46*, 3322−3356.

(26) Xu, Y.; Jin, S.; Xu, H.; Nagai, A.; Jiang, D. Conjugated Microporous Polymers: Design, Synthesis and Application. *Chem. Soc. Rev.* **2013**, *42*, 8012−8031.

(27) Jiang, J.-X.; Su, F.; Trewin, A.; Wood, C. D.; Campbell, N. L.; Niu, H.; Dickinson, C.; Ganin, A. Y.; Rosseinsky, M. J.; Khimyak, Y. Z.; Cooper, A. I. Conjugated Microporous Poly(aryleneethynylene) Networks. *Angew. Chem., Int. Ed.* **2007**, *46*, 8574−8578.

(28) Ben, T.; Qiu, S. Porous Aromatic Frameworks: Synthesis, Structure and Functions. *CrystEngComm* **2013**, *15*, 17−26.

(29) Huang, L.; Yang, X.; Cao, D. From Inorganic to Organic Strategy to Design Porous Aromatic Frameworks for High-Capacity Gas Storage. *J. Phys. Chem. C* **2015**, *119*, 3260−3267.

(30) Dutcher, B.; Fan, M.; Russell, A. G. Amine-Based CO_2 Capture Technology Development from the Beginning of 2013-A Review. *ACS Appl. Mater. Interfaces* **2015**, *7*, 2137−2148.

(31) Wu, S.; Gu, S.; Zhang, A.; Yu, G.; Wang, Z.; Jian, J.; Pan, C. A Rational Construction of Microporous Imide-Bridged Covalent-Organic Polytriazines for High-Enthalpy Small Gas Absorption. *J. Mater. Chem. A* **2015**, *3*, 878−885.

(32) Zhu, X.; Tian, C.; Veith, G. M.; Abney, C. W.; Dehaudt, J.; Dai, S. In Situ Doping Strategy for the Preparation of Conjugated Triazine Frameworks Displaying Efficient CO_2 Capture Performance. *J. Am. Chem. Soc.* **2016**, *138*, 11497−11500.

(33) Bhunia, A.; Vasylyeva, V.; Janiak, C. From a Supramolecular Tetranitrile to a Porous Covalent Triazine-Based Framework with High Gas Uptake Capacities. *Chem. Commun.* **2013**, *49*, 3961−3963.

(34) Park, K.; Lee, K.; Kim, H.; Ganesan, V.; Cho, K.; Jeong, S. K.; Yoon, S. Preparation of Covalent Triazine Frameworks with Imidazolium Cations Embedded in Basic Sites and their Application for CO_2 Capture. *J. Mater. Chem. A* **2017**, *5*, 8576−8582.

(35) Lu, W.; Yuan, D.; Sculley, J.; Zhao, D.; Krishna, R.; Zhou, H.-C. Sulfonate-Grafted Porous Polymer Networks for Preferential CO_2 Adsorption at Low Pressure. *J. Am. Chem. Soc.* **2011**, *133*, 18126−18129.

(36) Hussain, M. D. W.; Bandyopadhyay, S.; Patra, A. Microporous Organic Polymers Involving Thiadiazolopyridine for High and Selective Uptake of Greenhouse Gases at Low Pressure. *Chem. Commun.* **2017**, *53*, 10576−10579.

(37) Hug, S.; Mesch, M. B.; Oh, H.; Popp, N.; Hirscher, M.; Senker, J.; Lotsch, B. V. A Fluorene Based Covalent Triazine Framework with High CO_2 and H_2 Capture and Storage Capacities. *J. Mater. Chem. A* **2014**, *2*, 5928−5936.

(38) Katekomol, P.; Roeser, J.; Bojdys, M.; Weber, J.; Thomas, A. Covalent Triazine Frameworks Prepared from 1,3,5-Tricyanobenzene. *Chem. Mater.* **2013**, *25*, 1542−1548.

(39) Gu, C.; Liu, D.; Huang, W.; Liu, J.; Yang, R. Synthesis of Covalent Triazine-Based Frameworks with High CO_2 Adsorption and Selectivity. *Polym. Chem.* **2015**, *6*, 7410−7417.

(40) Bhunia, A.; Boldog, I.; Möller, A.; Janiak, C. Highly Stable Nanoporous Covalent Triazine-Based Frameworks with an Adamantane Core for Carbon Dioxide Sorption and Separation. *J. Mater. Chem. A* **2013**, *1*, 14990−14999.

(41) Liu, Y.; Wu, S.; Wang, G.; Yu, G.; Guan, J.; Pan, C.; Wang, Z. Control of Porosity of Novel Carbazole-Modified Polytriazine Frameworks for Highly Selective Separation of CO_2-N_2. *J. Mater. Chem. A* **2014**, *2*, 7795−7801.

(42) Wang, Y.; Li, J.; Yang, Q.; Zhong, C. Two-Dimensional Covalent Triazine Framework Membrane for Helium Separation and Hydrogen Purification. *ACS Appl. Mater. Interfaces* **2016**, *8*, 8694−8701.

(43) Rajendiran, S.; Park, K.; Lee, K.; Yoon, S. Ionic-Liquid-Based Heterogeneous Covalent Triazine Framework Cobalt Catalyst for the Direct Synthesis of Methyl 3-Hydroxybutyrate from Propylene Oxide. *Inorg. Chem.* **2017**, *56*, 7270−7277.

(44) Kamiya, K.; Tatebe, T.; Yamamura, S.; Iwase, K.; Harada, T.; Nakanishi, S. Selective Reduction of Nitrate by a Local Cell Catalyst Composed of Metal-Doped Covalent Triazine Frameworks. *ACS Catal.* **2018**, *8*, 2693−2698.

(45) Wang, T.; Kailasam, K.; Xiao, P.; Chen, G.; Chen, L.; Wang, L.; Li, J.; Zhu, J. Adsorption Removal of Organic Dyes on Covalent Triazine Framework (CTF). *Microporous Mesoporous Mater.* **2014**, *187*, 63−70.

(46) Leus, K.; Folens, K.; Nicomel, N. R.; Perez, J. P. H.; Filippousi, M.; Meledina, M.; Dîrtu, M. M.; Turner, S.; Tendeloo, G. V.; Garcia, Y.; Laing, G. D.; Van Der Voort, P. Removal of Arsenic and Mercury Species from Water by Covalent Triazine Framework Encapsulated γ-Fe_2O_3 Nanoparticles. *J. Hazard. Mater.* **2018**, *353*, 312−319.

(47) Li, Y.; Zheng, S.; Liu, X.; Li, P.; Sun, L.; Yang, R.; Wang, S.; Wu, Z.-S.; Bao, X.; Deng, W.-Q. Conductive Microporous Covalent Triazine-Based Framework for High-Performance Electrochemical Capacitive Energy Storage. *Angew. Chem., Int. Ed.* **2018**, *57*, 7992−7996.

(48) Hao, L.; Ning, J.; Luo, B.; Wang, B.; Zhang, Y.; Tang, Z.; Yang, J.; Thomas, A.; Zhi, L. Structural Evolution of 2D Microporous Covalent Triazine-Based Framework toward the Study of High-Performance Supercapacitors. *J. Am. Chem. Soc.* **2015**, *137*, 219−225.

(49) Gu, C.; Huang, N.; Gao, J.; Xu, F.; Xu, Y.; Jiang, D. Controlled Synthesis of Conjugated Microporous Polymer Films: Versatile Platforms for Highly Sensitive and Label-Free Chemo- and Biosensing. *Angew. Chem., Int. Ed.* **2014**, *53*, 4850−4855.

(50) Xiong, Y.; Qin, Y.; Su, L.; Ye, F. Bioinspired Synthesis of Cu^{2+}-Modified Covalent Triazine Framework: A New Highly Efficient and Promising Peroxidase Mimic. *Chem. - Eur. J.* **2017**, *23*, 11037−11045.

(51) Kuhn, P.; Thomas, A.; Antonietti, M. Toward Tailorable Porous Organic Polymer Networks: A High-Temperature Dynamic Polymerization Scheme Based on Aromatic Nitriles. *Macromolecules* **2009**, *42*, 319−326.

(52) Liebl, M. R.; Senker, J. Microporous Functionalized Triazine-Based Polyimides with High CO_2 Capture Capacity. *Chem. Mater.* **2013**, *25*, 970−980.

(53) Lee, Y. J.; Talapaneni, S. N.; Coskun, A. Chemically Activated Covalent Triazine Frameworks with Enhanced Textural Properties for High Capacity Gas Storage. *ACS Appl. Mater. Interfaces* **2017**, *9*, 30679−30685.

(54) Hug, S.; Tauchert, M. E.; Li, S.; Pachmayr, U. E.; Lotsch, B. V. A Functional Triazine Framework Based on *N*-Heterocyclic Building Blocks. *J. Mater. Chem.* **2012**, *22*, 13956−13964.

(55) Wang, G.; Leus, K.; Jena, H. S.; Krishnaraj, C.; Zhao, S.; Depauw, H.; Tahir, N.; Liu, Y.-Y.; Van Der Voort, P. A Fluorine-Containing Hydrophobic Covalent Triazine Framework with Excellent Selective CO_2 Capture Performance. *J. Mater. Chem. A* **2018**, *6*, 6370−6375.

(56) Hug, S.; Stegbauer, L.; Oh, H.; Hirscher, M.; Lotsch, B. V. Nitrogen-Rich Covalent Triazine Frameworks as High-Performance Platforms for Selective Carbon Capture and Storage. *Chem. Mater.* **2015**, *27*, 8001−8010.

(57) Tellez-Juárez, M. C.; Fierro, V.; Zhao, W.; Fernández-Huerta, N.; Izquierdo, M. T.; reguera, E.; Celzard, A. Hydrogen Storage in Activated Carbons Produced from Coals of Different Ranks: Effect of Oxygen Content. *Int. J. Hydrogen Energy* **2014**, *39*, 4996−5002.

(58) Blankenship, T. S., II; Balahmar, N.; Mokaya, R. Oxygen-Rich Microporous Carbons with Exceptional Hydrogen Storage Capacity. *Nat. Commun.* **2017**, *8*, No. 1545.

(59) Lee, H. M.; Youn, I. S.; Saleh, M.; Lee, J. W.; Kim, K. S. Interactions of CO_2 with Various Functional Molecules. *Phys. Chem. Chem. Phys.* **2015**, *17*, 10925−10933.

(60) Meldal, M.; Tornøe, C. W. Cu-Catalyzed Azide−Alkyne Cycloaddition. *Chem. Rev.* **2008**, *108*, 2952−3015.

(61) Kuhn, P.; Antonietti, M.; Thomas, A. Porous, Covalent Triazine-Based Frameworks Prepared by Ionothermal Synthesis. *Angew. Chem., Int. Ed.* **2008**, *47*, 3450−3453.

(62) Wang, X.-J.; Li, P.-Z.; Chen, Y.; Zhang, Q.; Zhang, H.; Chan, X. X.; Ganguly, R.; Li, Y.; Jiang, J.; Zhao, Y. A Rationally Designed Nitrogen-Rich Metal-Organic Framework and Its Exceptionally High CO_2 and H_2 Uptake Capability. *Sci. Rep.* **2013**, *3*, No. 1149.

(63) Hu, X.-M.; Chen, Q.; Zhao, Y.-C.; Laursen, B. W.; Han, B.-H. Straightforward Synthesis of a Triazine-Based Porous Carbon with High Gas-Uptake Capacities. *J. Mater. Chem. A* **2014**, *2*, 14201−14208.

(64) Saleh, M.; Baek, S. B.; Lee, H. M.; Kim, K. S. Triazine-Based Microporous Polymers for Selective Adsorption of CO_2. *J. Phys. Chem. C* **2015**, *119*, 5395−5402.

(65) Pandey, P.; Farha, O. K.; Spokoyny, A. M.; Mirkin, C. A.; Kanatzidis, M. G.; Hupp, J. T.; Nguyen, S. T. A "Click-Based" Porous Organic Polymer from Tetrahedral Building Blocks. *J. Mater. Chem.* **2011**, *21*, 1700−1703.

(66) Zhong, H.; Liu, C.; Wang, Y.; Wang, R.; Hong, M. Tailor-Made Porosities of Fluorene-Based Porous Organic Frameworks for the Pre-Designable Fabrication of Palladium Nanoparticles with Size, Location and Distribution Control. *Chem. Sci.* **2016**, *7*, 2188−2194.

(67) Mukherjee, S.; Monojit Das, M.; Anupam Manna, A.; Rajamani Krishna, R.; Das, S. Newly Designed 1,2,3-Triazole Functionalized Covalent Triazine Frameworks with Exceptionally High Uptake Capacity for both CO_2 and H_2. *J. Mater. Chem. A* **2019**, *7*, 1055−1068.

(68) Dey, S.; Bhunia, A.; Breitzke, H.; Groszewicz, P. B.; Buntkowsky, G.; Janiak, C. A Mixed-Linker Approach Towards Improving Covalent Triazine-Based Frameworks for CO_2 Capture and Separation. *J. Mater. Chem. A* **2017**, *5*, 3609−3620.

(69) Kuhn, P.; Forget, A.; Su, D.; Thomas, A.; Antonietti, M. From Microporous Regular Frameworks to Mesoporous Materials with Ultrahigh Surface Area: Dynamic Reorganization of Porous Polymer Networks. *J. Am. Chem. Soc.* **2008**, *130*, 13333−13337.

(70) Kuhn, P.; Forget, A.; Hartmann, J.; Thomas, A.; Antonietti, M. Template-Free Tuning of Nanopores in Carbonaceous Polymers through Ionothermal Synthesis. *Adv. Mater.* **2009**, *21*, 897−901.

(71) Johns, I. B.; Moelhill, E. A.; Smith, J. O. Thermal Stability of Organic Compounds. *Ind. Eng. Chem. Prod. Res. Dev.* **1962**, *1*, 2−6.

(72) Marchon, B.; Carrazza, J.; Heinemann, H.; Somorjai, G. A. TPD and XPS Studies of O_2, CO_2, and H_2O Adsorption on Clean Polycrystalline Graphite. *Carbon* **1988**, *26*, 507−514.

(73) Pehrsson, P. E.; Zhao, W.; Baldwin, J. W.; Chulho Song, C.; Jie Liu, J.; Steven Kooi, S.; Bo Zheng, B. Thermal Fluorination and Annealing of Single-Wall Carbon Nanotubes. *J. Phys. Chem. B* **2003**, *107*, 5690−5695.

(74) Gu, J.-M.; Kim, W.-S.; Hwang, Y.-K.; Huh, S. Template-Free Synthesis of N-Doped Porous Carbons and their Gas Sorption Properties. *Carbon* **2013**, *56*, 208−217.

(75) Chen, G.; Wang, X.; Li, J.; Hou, W.; Zhou, Y.; Wang, J. Direct Carbonization of Cyanopyridinium Crystalline Dicationic Salts into Nitrogen-Enriched Ultra-Microporous Carbons toward Excellent CO_2 Adsorption. *ACS Appl. Mater. Interfaces* **2015**, *7*, 18508−18518.

(76) León, V.; Quintana, M.; Herrero, M. A.; Fierro, J. L. G.; de la Hoz, A.; Prato, M.; Vázquez, E. Few-Layer Graphenes from Ball-Milling of Graphite with Melamine. *Chem. Commun.* **2011**, *47*, 10936−10938.

(77) Osadchii, D. Y.; Olivos-Suarez, A. I.; Bavykina, A. V.; Gascon, J. Revisiting Nitrogen Species in Covalent Triazine Frameworks. *Langmuir* **2017**, *33*, 14278−14285.

(78) Ciampi, S.; Böcking, T.; Kilian, K. A.; James, M.; Harper, J. B.; Gooding, J. J. Functionalization of Acetylene-Terminated Monolayers on Si(100) Surfaces: A Click Chemistry Approach. *Langmuir* **2007**, *23*, 9320−9329.

(79) Briggs, D.; Beamson, G. XPS Studies of the Oxygen 1s and 2s Levels in a Wide Range of Functional Polymers. *Anal. Chem.* **1993**, *65*, 1517−1523.

(80) Zhao, Z.; Dai, Y.; Lin, J.; Wang, G. Highly-Ordered Mesoporous Carbon Nitride with Ultrahigh Surface Area and Pore Volume as a Superior Dehydrogenation Catalyst. *Chem. Mater.* **2014**, *26*, 3151−3161.

(81) Ferrari, A. C.; Robertson, J. Resonant Raman spectroscopy of disordered, amorphous, and diamondlike carbon. *Phys. Rev. B* **2001**, *64*, No. 075414.

(82) Kaufman, J. H.; Metin, S.; Saperstein, D. D. Symmetry breaking in nitrogen-doped amorphous carbon: Infrared observation of the Raman-active *G* and *D* bands. *Phys. Rev. B* **1989**, *39*, 13053−13060.

(83) Talapaneni, S. N.; Lee, J. H.; Je, S. H.; Buyukcakir, O.; Kwon, T.; Polychronopoulou, K.; Choi, J. W.; Coskun, A. Chemical Blowing Approach for Ultramicroporous Carbon Nitride Frameworks and Their Applications in Gas and Energy Storage. *Adv. Funct. Mater.* **2017**, *27*, No. 1604658.

(84) Liu, X.; Li, H.; Zhang, Y.; Xu, B.; Sigen, A.; Xia, H.; Mu, Y. Enhanced Carbon Dioxide Uptake by Metalloporphyrin-Based Microporous Covalent Triazine Framework. *Polym. Chem.* **2013**, *4*, 2445−2448.

(85) Bojdys, M. J.; Jeromenok, J.; Thomas, A.; Antonietti, M. Rational Extension of the Family of Layered, Covalent, Triazine-Based Frameworks with Regular Porosity. *Adv. Mater.* **2010**, *22*, 2202−2205.

(86) Thommes, M.; Kaneko, K.; Neimark, A. V.; Olivier, J. P.; Rodriguez-Reinoso, F.; Rouquerol, J.; Sing, K. S. W. Physisorption of Gases, with Special Reference to the Evaluation of Surface Area and Pore Size Distribution (IUPAC Technical Report). *Pure Appl. Chem.* **2015**, *87*, 1051−1069.

(87) Sing, K. S. W.; Everett, D. H.; Haul, R. A. W.; Moscou, L.; Pierotti, R. A.; Rouquerol, J.; Siemieniewska, T. Reporting Physisorption Data for Gas/Solid Systems with Special Reference to the Determination of Surface Area and Porosity. *Pure Appl. Chem.* **1985**, *57*, 603−619.

(88) Gil, A.; Korili, S. A.; Vicente, M. A. Recent Advances in the Control and Characterization of the Porous Structure of Pillared Clay Catalysts. *Catal. Rev.* **2008**, *50*, 153−221.

(89) Zhu, Y.; Long, H.; Zhang, W. Imine-Linked Porous Polymer Frameworks with High Small Gas (H_2, CO_2, CH_4, C_2H_2) Uptake and CO_2/N_2 Selectivity. *Chem. Mater.* **2013**, *25*, 1630−1635.

(90) Jin, T.; Xiong, Y.; Zhu, X.; Tian, Z.; Tao, D.-J.; Hu, J.; Jiang, D.-E.; Wang, H.; Liu, H.; Dai, S. Rational Design and Synthesis of a Porous, Task-Specific Polycarbazole For Efficient CO_2 Capture. *Chem. Commun.* **2016**, *52*, 4454−4457.

(91) Arab, P.; Rabbani, M. G.; Sekizkardes, A. K.; İslamoğlu, T.; El-Kaderi, H. M. Copper(I)-Catalyzed Synthesis of Nanoporous Azo-Linked Polymers: Impact of Textural Properties on Gas Storage and Selective Carbon Dioxide Capture. *Chem. Mater.* **2014**, *26*, 1385−1392.

(92) Hao, G.-P.; Li, W.-C.; Qian, D.; Lu, A.-H. Rapid Synthesis of Nitrogen-Doped Porous Carbon Monolith for CO_2 Capture. *Adv. Mater.* **2010**, *22*, 853−857.

(93) Cazorla-Amorós, D.; Alcañiz-Monge, J.; Linares-Solano, A. Characterization of Activated Carbon Fibers by CO_2 Adsorption. *Langmuir* **1996**, *12*, 2820−2824.

(94) Abdelmoaty, Y. H.; Tessema, T.-D.; Choudhury, F. A.; El-Kadri, O.-M.; El-Kaderi, H. M. Nitrogen-Rich Porous Polymers for Carbon Dioxide and Iodine Sequestration for Environmental Remediation. *ACS Appl. Mater. Interfaces* **2018**, *10*, 16049−16058.

(95) Buyukcakir, O.; Yuksel, R.; Jiang, Y.; Lee, S. H.; Seong, W. K.; Chen, X.; Ruoff, R. S. Synthesis of Porous Covalent Quinazoline Networks (CQNs) and Their Gas Sorption Properties. *Angew. Chem., Int. Ed.* **2019**, *58*, 872−876.

(96) Tuci, G.; Pilaski, M.; Ba, H.; Rossin, A.; Luconi, L.; Caporali, S.; Pham-Huu, C.; Palkovits, R.; Giambastiani, G. Unraveling Surface

Basicity and Bulk Morphology Relationship on Covalent Triazine Frameworks with Unique Catalytic and Gas Adsorption Properties. *Adv. Funct. Mater.* **2017**, *27*, No. 1605672.

(97) Gómez-Gualgrón, D. A.; Colón, Y. J.; Zhang, X.; Wang, T. C.; Chen, Y.-S.; Hupp, J.-T.; Yildirim, T.; Farha, O. K.; Zhang, J.; Snurr, R. Q. Evaluating Topologically Diverse Metal-Organic Frameworks for Cryo-Adsorbed Hydrogen Storage. *Energy. Environ. Sci.* **2016**, *9*, 3279−3289.

(98) Chen, Q.; Luo, M.; Hammershøj, M. P.; Zhou, D.; Han, Y.; Laursen, B. W.; Yan, C.-G.; Han, B.-H. Microporous Polycarbazole with High Specific Surface Area for Gas Storage and Separation. *J. Am. Chem. Soc.* **2012**, *134*, 6084−6087.

(99) Chen, Q.; Liu, D.-P.; Zhu, J.-H.; Han, B.-H. Mesoporous Conjugated Polycarbazole with High Porosity via Structure Tuning. *Macromolecules* **2014**, *47*, 5926−5931.

(100) Li, G.; Zhang, B.; Yan, J.; Wang, Z. Tetraphenyladamantane-Based Polyaminals for Highly Efficient Captures of CO_2 and Organic Vapors. *Macromolecules* **2014**, *47*, 6664−6670.

(101) Mohanty, P.; Kull, L. D.; Landskron, K. Porous Covalent Electron-Rich Organonitridic Frameworks as Highly Selective Sorbents for Methane and Carbon Dioxide. *Nat. Commun.* **2011**, *2*, No. 401.

(102) Walton, K. S.; Sholl, D. S. Predicting Multicomponent Adsorption: 50 Years of the Ideal Adsorbed Solution Theory. *AIChE J.* **2015**, *61*, 2757−2762.

(103) Miltner, M.; Makaruk, A.; Harasek, M. Review on Available Biogas Upgrading Technologies and Innovations towards Advanced Solutions. *J. Cleaner Prod.* **2017**, *161*, 1329−1337.

(104) Baker, R. W. *Membrane Technology and Applications*, 2nd ed.; Wiley: New York, 2004.

(105) Krishna, R.; Long, J. R. Screening Metal-Organic Frameworks by Analysis of Transient Breakthrough of Gas Mixtures in a Fixed Bed Adsorber. *J. Phys. Chem. C* **2011**, *115*, 12941−12950.

(106) Krishna, R. The Maxwell-Stefan Description of Mixture Diffusion in Nanoporous Crystalline Materials. *Microporous Mesoporous Mater.* **2014**, *185*, 30−50.

(107) Krishna, R. Methodologies for Evaluation of Metal-Organic Frameworks in Separation Applications. *RSC Adv.* **2015**, *5*, 52269−52295.

(108) Krishna, R. Screening Metal-Organic Frameworks for Mixture Separations in Fixed-Bed Adsorbers Using a Combined Selectivity/Capacity Metric. *RSC Adv.* **2017**, *7*, 35724−35737.

(109) Huang, N.; Krishna, R.; Jiang, D. Tailor-Made Pore Surface Engineering in Covalent Organic Frameworks: Systematic Functionalization for Performance Screening. *J. Am. Chem. Soc.* **2015**, *137*, 7079−7082.

(110) Zhao, Y.; Yao, K. X.; Teng, B.; Zhang, T.; Han, Y. A Perfluorinated Covalent Triazine-Based Framework for Highly Selective and Water-Tolerant CO_2 Capture. *Energy Environ. Sci.* **2013**, *6*, 3684−3692.

DOI: 10.1021/acs.chemmater.8b05365
Chem. Mater. 2019, 31, 3929−3940

Dual Strategic Approach to Prepare Defluorinated Triazole Embedded Covalent Triazine Frameworks with High Gas Uptake Performance

Soumya Mukherjee,[ab] Monojit Das,[ab] Anupam Manna,[ab] Rajamani Krishna,[c] and Sanjib Das*[ab]

[a]Department of Colloids & Materials Chemistry, CSIR-Institute of Minerals & Materials Technology, Bhubaneswar 751013, India.

[b]Academy of Scientific & Innovative Research (AcSIR), Ghaziabad 201002, India.

[c]Van‘t Hoff Institute for Molecular Sciences, University of Amsterdam, Science Park 904,
1098 XH Amsterdam, The Netherlands.

Corresponding Author: sanjibdas@immt.res.in

Section A. Materials and Methods:

All chemical reagents were purchased from commercial sources and used as received unless otherwise stated. Periodic acid, potassium iodide, triethylamine, cesium fluoride, copper sulphate pentahydrate and sodium thiosulfate were purchased from Spectrochem, India. 1,3,5-trifluorobenzene, 1,3,5-tribromobenzene, pentafluorobenzonitrile, (trimethylsilyl)acetylene, tetrakis(triphenylphosphine)palladium(0) and sodium ascorbate were purchased from Alfa-Aesar. Anhydrous zinc chloride was purchased from Alfa-Aesar and further dried at 110 ^{0}C under vacuum prior to use. Column chromatography was performed using silica gel purchased from Spectrochem, India. All organic solvents were procured from Spectrochem, India. Anhydrous THF was prepared by freshly distilled from continuously refluxing THF over sodium under argon. Triethylamine was purified prior to use via distillation over KOH.

Solution ^{1}H, and ^{19}F NMR spectra were recorded on a Bruker® Ultrashield instrument operating at a frequency of 400 MHz with tetramethylsilane (TMS) as an internal standard using deuterated $CDCl_3$ or DMSO as solvent. All measurements were carried out at ambient temperature and chemical shifts are reported in parts per million (ppm) relative to the deuterated solvent. Fourier-transform Infrared spectra (FT-IR) of starting materials and as-synthesized Tz-*df*-CTFs materials were obtained using a Perkin Elmer Spectrum-GX spectrophotometer with KBr pallet in transmittance mode. All FT-IR spectra were background corrected. Powder X-ray diffraction (PXRD) patterns were recorded on a Rigaku Ultima-IV diffractometer using monochromatic Cu-K_α ($\lambda = 1.54060$ Å) radiation with a scan speed of 2° min^{-1} and a step size of 0.01° in 2θ. The X-ray tube operated at a voltage of 40 kV and a current of 30 mA. Thermogravimetric analyses were carried out in a nitrogen stream using Netzsch STA 449F3-jupiter thermogravimetric-differential scanning calorimetry (TG-DSC) analyzer with a heating rate of 10 °C/min. The Raman spectra were measured on a Horiba LabRAM HR confocal micro-Raman system with an excitation source of 532 nm diode-pumped solid-state laser. Field emission scanning electron microscopy (FE-SEM) images were taken using Carl Zeiss AG Supra Gemini 55 at an accelerating voltage of 15 kV and equipped with OXFORD energy dispersive X-ray spectrometer. The powder samples were dispersed in ethanol and the suspension was drop cast on a clean piece of silicon wafer. High resolution transmission electron microscopy (HR-TEM) images were captured using field-emission JEOL, JEM-2100F instrument. The powder samples were dispersed in chloroform and one drop of the suspension was drop cast on a carbon-coated copper grid.

Elemental analysis (C, H, and N) were performed on a Thermo Scientific Flash 2000 Organic Elemental Analyzer. High resolution X-ray photoelectron spectroscopy (XPS) spectra were recorded with PHI 5000 Versa Probe II XPS with AES module comprising argon ion as well as C60 sputter guns.

Gas adsorption-desorption experiments (up to 1 bar) were carried out on Quantachrome Autosorb-iQ surface area & pore size analyzer. Before gas adsorption experiment sample was degassed first at 140°C under a dynamic vacuum for 12 hours. High-purity-grade He, N_2, H_2, CO_2 and CH_4 gases were used in all adsorption measurements. The N_2 (77 K) and H_2 (77 K) isotherms were measured using a liquid nitrogen bath. The CO_2 and CH_4 isotherms measured at 273 K and 298 K using a jacketed recirculating dewar containing mixed water and ethylene glycol (1:1 ratio) and the dewar was connected to a chiller (JULABO, FL300, working temperature range: -20 to +40°C, temperature stability: ± 0.5 °C) having circulating methanol to precisely achieve the isothermal condition during measurement. The Brunauer-Emmett-Teller (BET) surface area was calculated over the relative pressure range 0.05 – 0.3 P/P_0 whereas Langmuir surface area calculated taking relative pressure range 0 – 0.15 P/P_0. Total pore volumes were measured at relative pressure near 0.99 P/P_0 while microporosity was estimated by measuring the pore volume at a relative pressure of 0.1 P/P_0. Pore size distributions and pore volumes were derived from both N_2 (77 K) and CO_2 (273 K) adsorption-desorption isotherms using the classical t-plot method as well as non-local density functional theory (NL-DFT) slit-pore model for porous carbon using ASiQwin software package. High pressure gas adsorption analysis was performed using fully automated volumetric gas sorption analyzer namely iSorb-HP1 (Model-iSorbHP1-XKRHSPNF100) from Quantachrome Instrument, USA using Polyscience circulator (serial no.1C1482229) to maintain the required isothermal condition during gas adsorption analysis.

Section B. General Synthetic Procedure of Precursors:

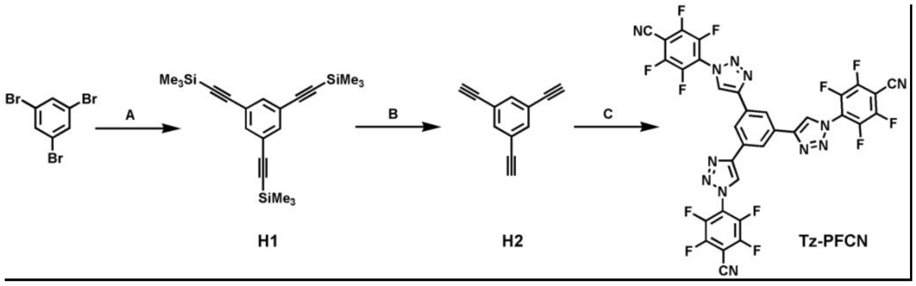

A: Trimethylsilylacetylene, CuI, $Pd(PPh_3)_4$, THF, Triethylamine, 70°C, Overnight; **B**: CsF, Ethanol, Tetrahydrofuran, 50 min, RT; **C:** 4-Azidotetrafluorobenzonitrile, Sodium ascorbate, Water, Tetrahydrofuran, 60°C, 3 days.

Scheme S1: Synthetic route of Tz-PFCN building block.

1,3,5-tris[2-(trimethylsilyl)ethynyl]benzene:[S1] A 250 ml two neck round bottom flask equipped with stir bar was charged with 1,3,5-tribromobenzne (6.0 g, 19.05 mmol), CuI (145.12 mg, 0.762 mmol), PPh_3 (999.32 mg, 3.81 mmol), $PdCl_2(PPh_3)_2$ (668.56 mg, 0.95 mmol), anhydrous THF (60 ml), and triethylamine (60 ml). The mixture was purged with argon over 10 mins at room temperature followed by dropwise addition of trimethylsilylacetylene (6.74 g, 19.05 mmol) under inert condition. The reaction mixture was heated to 70^{o}C for overnight and cooled down to room temperature. The mixture was filtered and the filtrate was extracted by chloroform (3 x 50 ml) and washed with water and then dried over anhydrous $MgSO_4$. Organic layer was evaporated to dryness and the crude product was purified via column chromatography (silica gel, hexane) to obtain cream colored solid compound (5.3 g, 80%). ^{1}H NMR (400 MHz; $CDCl_3$): 0.23 (s, 27H), 7.49 (s, 3H).

1,3,5-triethynylbenzene:[S2] A 50 ml round bottom flask equipped with stir bar was charged with 1,3,5-tris[2-(trimethylsilyl)ethynyl]benzene **H1** (2 g, 5.45 mmol), tetrahydrofuran (30 ml) and ethanol (15 ml) followed by addition of CsF (2.60 g, 17.18 mmol). The reaction mixture was then stirred for 50 minutes under inert condition at RT. It was filtered then and solvent was evaporated under reduced pressure and the crude product was purified by silica gel column chromatography (petroleum ether) to obtain the white colored pure compound **H2** (750 mg, 91.6% yield). ^{1}H NMR (400 MHz; $CDCl_3$): 3.11 (s, 3H), 7.57 (s, 3H).

Section C. ^{1}H and ^{19}F NMR Spectroscopy Studies:

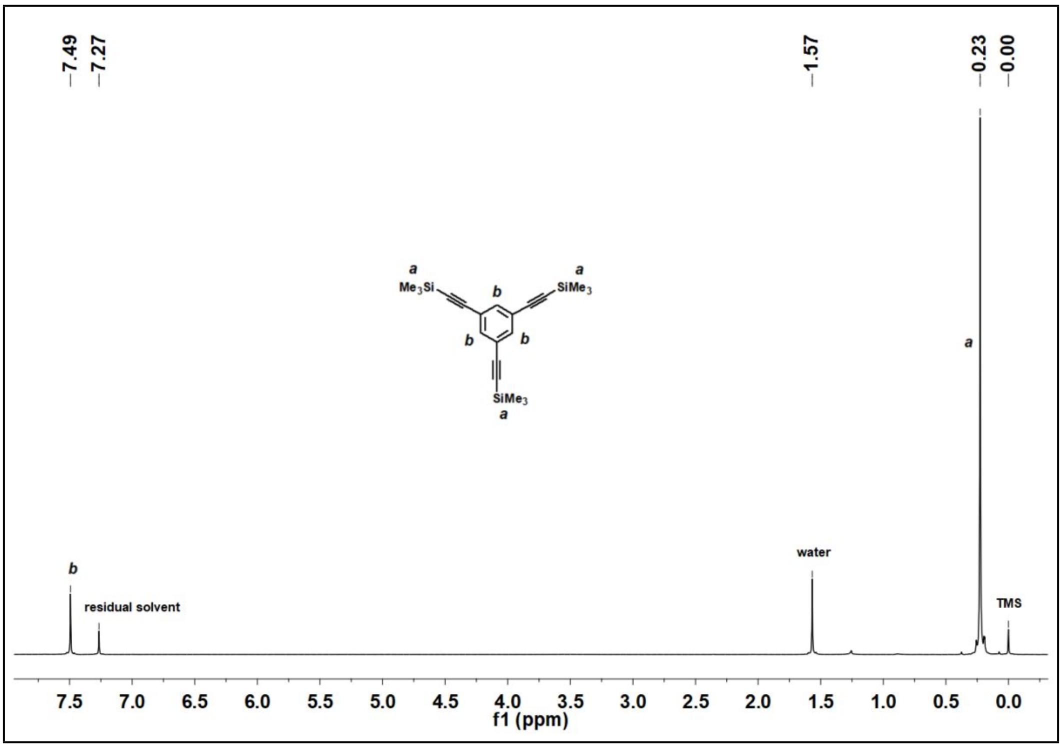

Figure S1: ^{1}H NMR of 1,3,5-tris[2-(trimethylsilyl)ethynyl]benzene

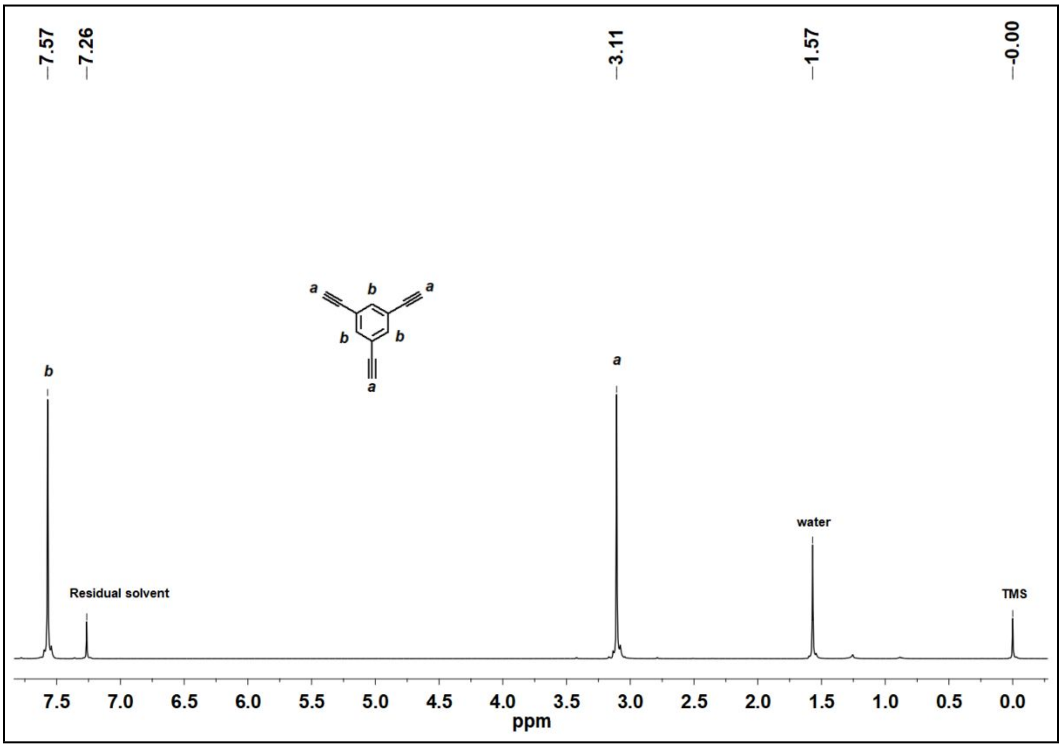

Figure S2: ^{1}H NMR of 1,3,5-triethynylbenzene

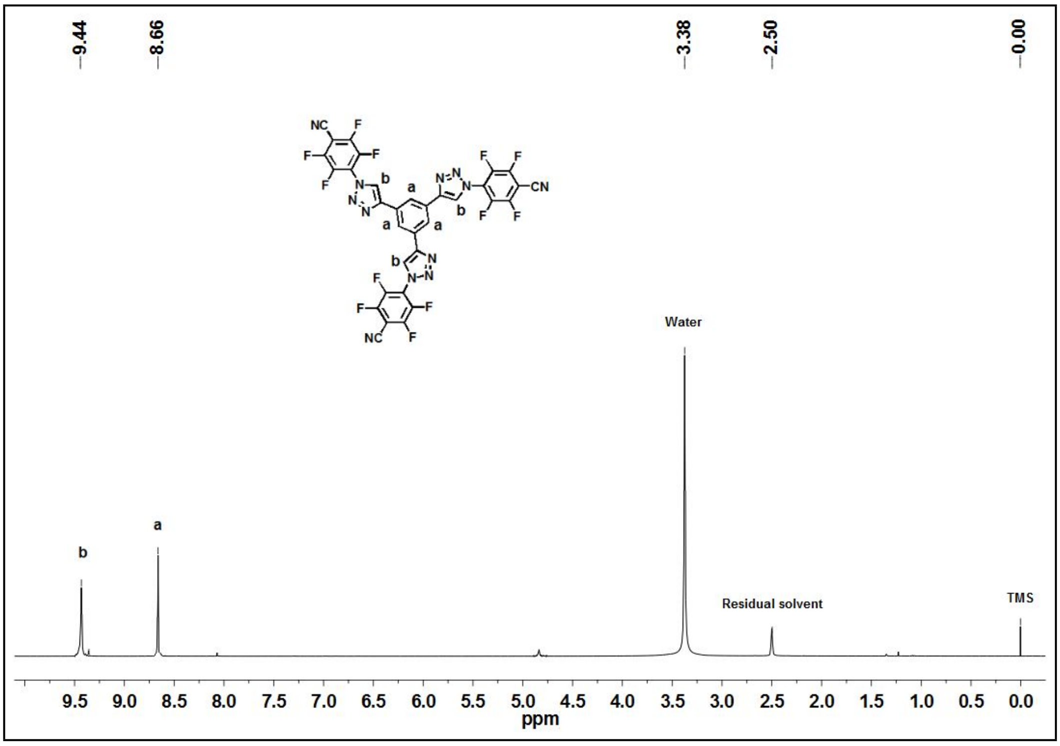

Figure S3: ^{1}H NMR of Tz-PFCN building block

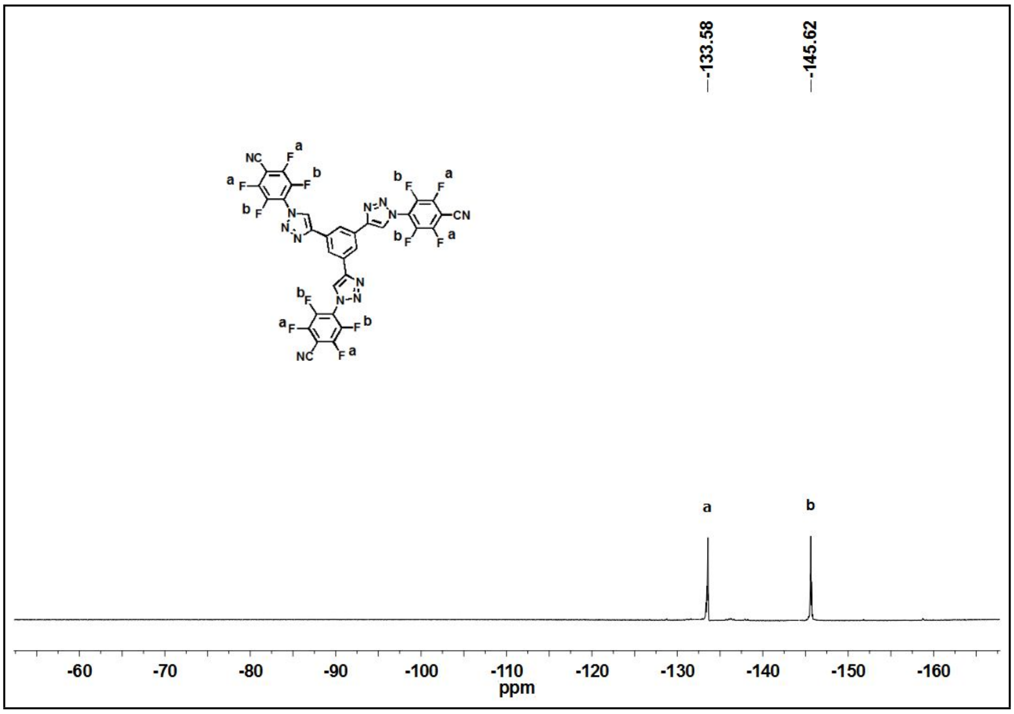

Figure S4: ^{19}F NMR of Tz-PFCN building block

Section D. Elemental Analysis:

Table S1. Elemental analysis of Tz-*df*-CTF materials from combustion process

Sample	Elemental Analysis (Experimental)			C/N	C/H
	C	N	H		
Tz-*df*-CTF400	49.39	9.63	1.74	5.12	28.38
Tz-*df*-CTF500	47.90	7.97	2.04	6.01	23.48
Tz-*df*-CTF600	48.39	6.15	2.25	7.86	21.50
Calc. Tz-PFCN	49.64	21.05	0.76	2.35	65.31

Section E. XPS Survey Scan of Tz-*df*-CTFs:

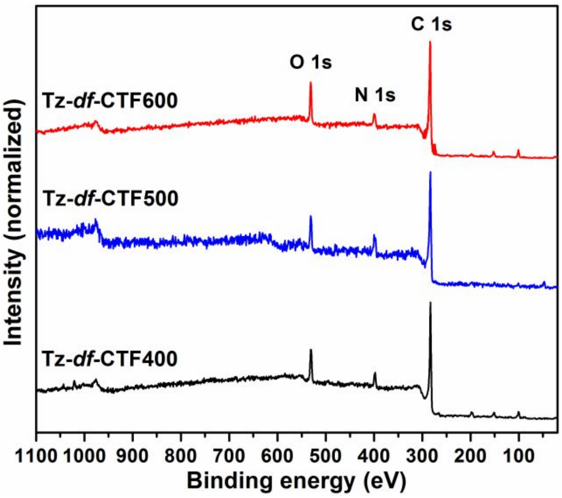

Figure S5: XPS survey spectra Tz-*df*-CTFs

Section F. Wide-Angle Powder XRD Analysis of Tz-*df*-CTFs:

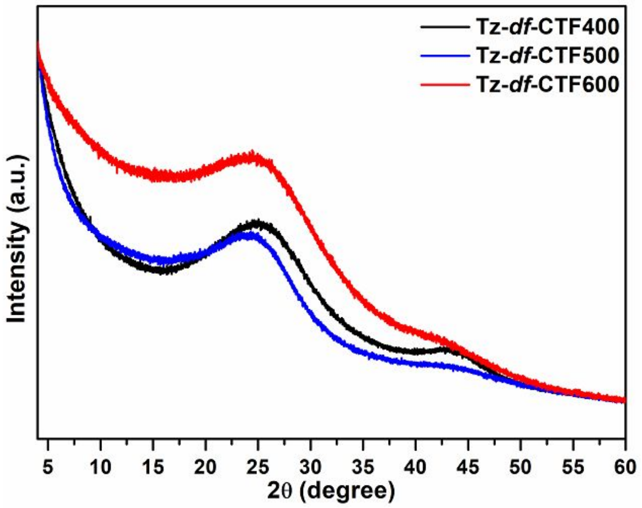

Figure S6. Powder X-ray diffraction spectra of Tz-*df*-CTFs.

Section G. FE-SEM and HRTEM Analysis of Tz-*df*-CTFs:

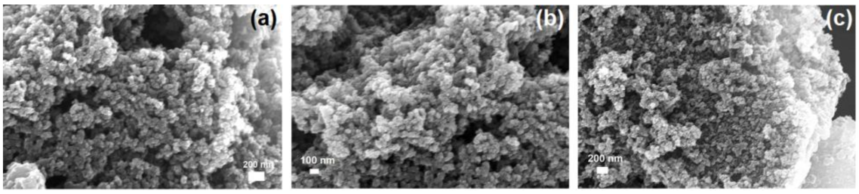

Figure S7. FE-SEM images of (a) Tz-*df*-CTF400, (b) Tz-*df*-CTF500, and (c) Tz-*df*-CTF600.

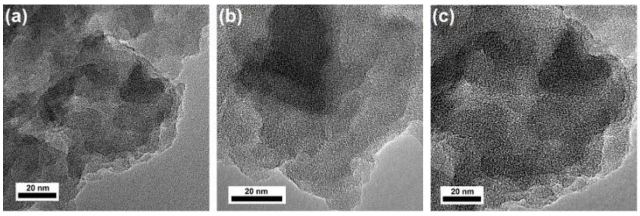

Figure S8. HR-TEM image (a) Tz-*df*-CTF400, (b) Tz-*df*-CTF500, and (c) Tz-*df*-CTF600.

Section H. Pore Size Distribution Curves Derived from CO_2 Isotherm:

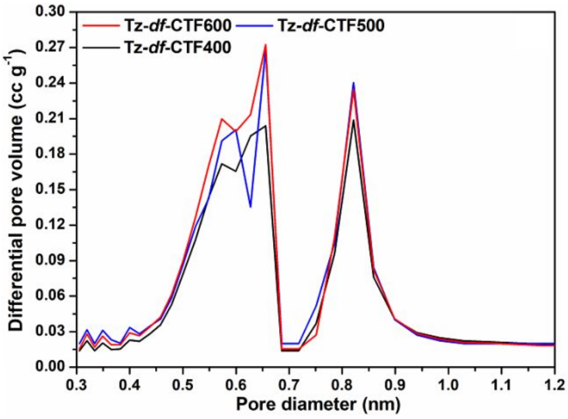

Figure S9. Pore size distribution curve of Tz-*df*-CTFs derived from CO_2 adsorption isotherms (273 K) using NL-DFT method.

Section I. Fitting of Unary Isotherm Data:

The unary isotherm data for CO_2, CH_4, and N_2, measured at 273 K and 298 K in Tz-*df*-CTFs, were fitted with excellent accuracy with the single-site Langmuir isotherm model

$$q = q_{sat} \frac{bp}{1+bp} \tag{1}$$

with *T*-dependent parameter *b*

$$b = b_0 \exp\left(\frac{E}{RT}\right) \tag{2}$$

The fitted parameter values are presented in **Table S2**,

Table S3, and **Table S4** derived from unary gas isotherm data of all Tz-*df*-CTFs measured at 273 K and 298 K.

Table S2. Langmuir fit parameter values for CO_2, CH_4, and N_2 in Tz-*df*-CTF400.

Gas	q_{sat} **(mol kg^{-1})**	b_0 **(Pa^{-1})**	*E* **(kJ mol^{-1})**
CO_2	8.5	8.42E-10	23.4
CH_4	5.4	4.04E-11	27.4
N_2	12.6	3.32E-11	23.2

Table S3. Langmuir fit parameter values for CO_2, CH_4, and N_2 in Tz-*df*-CTF500.

Gas	q_{sat} **(mol kg^{-1})**	b_0 **(Pa^{-1})**	*E* **(kJ mol^{-1})**
CO_2	11	2.90E-09	19.7
CH_4	11	1.51E-10	22.5
N_2	15	3.10E-12	28.6

Table S4. Langmuir fit parameter for CO_2, CH_4, and N_2 in Tz-*df*-CTF600.

Gas	q_{sat} **(mol kg^{-1})**	b_0 **(Pa^{-1})**	*E* **(kJ mol^{-1})**
CO_2	11.6	2.48E-09	20
CH_4	7.1	1.57E-10	24
N_2	15	1.01E-11	26

Section J. Isosteric Heat of Adsorption:

The isosteric heat of adsorption, Q_{st}, defined as

$$Q_{st} = RT^2 \left(\frac{\partial \ln p}{\partial T}\right)_q \tag{3}$$

were determined from the pure component isotherm fits at 298 K and 273 K using the Clausius-Clapeyron equation.

Section K. IAST Calculation of Component Uptakes and Adsorption Selectivities:

The IAST calculations were performed for binary 15/85 CO_2/N_2 and 50/50 CO_2/CH_4 gas mixtures at 298 K. The adsorption selectivity was calculated using equation

$$S_{ads} = \frac{q_A/q_B}{y_A/y_B} \qquad (1)$$

where the q_A, and q_B represent the molar loadings of Tz-*df*-CTFs that is in equilibrium with a bulk fluid mixture with mole fractions y_A, and $y_B = 1 - y_A$. The molar loadings, also called gravimetric uptake capacities, are expressed in mol kg^{-1}. For 15/85 CO_2/N_2 separations, the mole fractions $y_A = 0.15$ and $y_B = 1 - y_A = 0.85$. For 50/50 CO_2/CH_4 separations, the mole fractions $y_A = 0.5$ and $y_B = 1 - y_A = 0.5$.

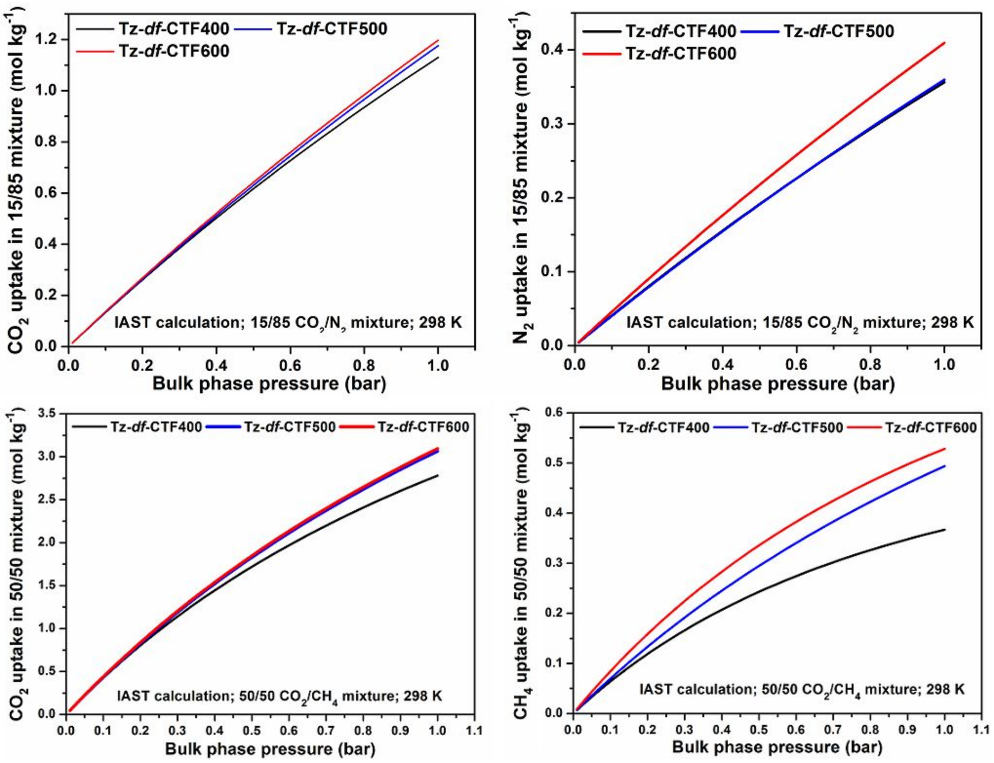

Figure S10. Calculations using Ideal Adsorbed Solution Theory (IAST) for uptakes of CO_2, CH_4 and N_2, expressed as moles per kg of adsorbent, in equilibrium with binary CO_2/N_2 as well as CO_2/CH_4 gas mixture maintained at isothermal condition at 298 K. In these calculations the partial pressures of CO_2 and N_2 for CO_2/N_2 mixture are taken to be p_1/p_2 = 15/85 and p_1/p_2 = 50/50 for CO_2/CH_4 mixture

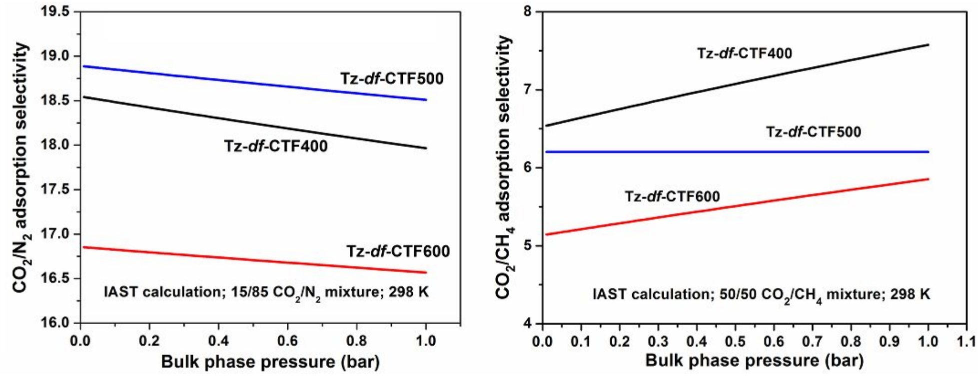

Figure S11. Calculations using Ideal Adsorbed Solution Theory (IAST) for CO_2/N_2 and CO_2/CH_4 adsorption selectivity for a binary CO_2/N_2 and CO_2/CH_4 gas mixture and maintained at isothermal condition at 298 K. In these calculations the partial pressures of CO_2 and N_2 are taken to be $p_1/p_2 = 15/85$ and for CO_2 and CH_4 are taken to be $p_1/p_2 = 50/50$

Section L. Transient Breakthrough of mixtures in Fixed Bed Adsorbers:

The performance of industrial fixed bed adsorbers is dictated by a combination of adsorption selectivity and uptake capacity. Transient breakthrough simulations were carried out for binary 15/85 CO_2/N_2 and 50/50 CO_2/CH_4 gas mixtures operating at a total pressure of 100 kPa and 298 K, using the simulation methodology described in earlier publications as stated in main text. In a typical breakthrough simulation, the following parameter values were used: length of packed bed, $L = 0.3$ m; voidage of packed bed, $\varepsilon = 0.4$; superficial gas velocity at inlet, $u = 0.04$ m/s. The transient breakthrough simulation results are presented in terms of a *dimensionless* time, $\tau = \frac{tu}{L\varepsilon}$. The y-axis is % of component in the gas mixture exiting the adsorber. The partial pressures of CO_2 and N_2 in 15/85 CO_2/N_2 binary gas mixture at the feed gas inlet are 15 kPa, and 85 kPa, respectively. Similarly, the partial pressures of CO_2 and CH_4 in 50/50 CO_2/ CH_4 binary mixture at the feed gas inlet are 50 kPa, and 50 kPa, respectively.

Section M. Henry Selectivity Studies:

Table S5. Initial Slopes for individual isotherm and Henry Selectivity of Tz-*df*-CTFs.

Temp.	Initial slope								
	Tz-*df*-CTF400			Tz-*df*-CTF500			Tz-*df*-CTF600		
	CO_2	CH_4	N_2	CO_2	CH_4	N_2	CO_2	CH_4	N_2
273K	19.331	4.072	1.139	20.986	3.439	1.444	21.594	4.301	1.418
298K	11.468	1.425	0.504	11.260	1.562	0.524	11.142	1.941	0.528

Temp.	Henry selectivity					
	Tz-*df*-CTF400		Tz-*df*-CTF500		Tz-*df*-CTF600	
	CO_2/CH_4	CO_2/N_2	CO_2/CH_4	CO_2/N_2	CO_2/CH_4	CO_2/N_2
273K	4.747	16.971	6.102	14.533	5.021	15.228

298K	8.047	22.754	7.208	21.488	5.740	21.102

Section N. Henry Plot for CO_2, N_2, and CH_4:

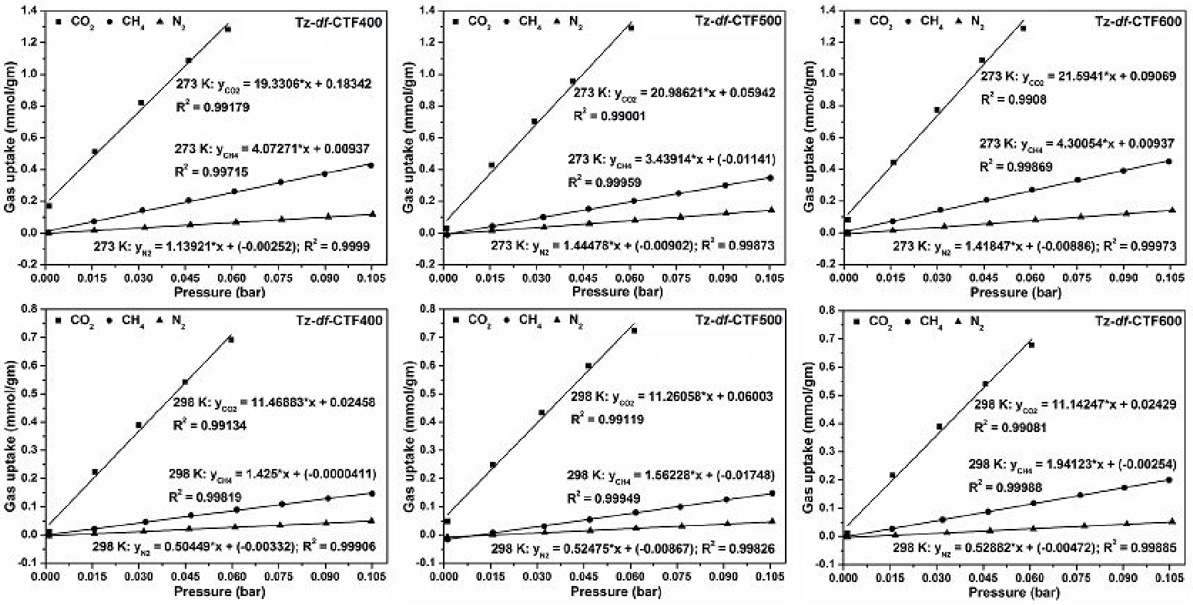

Figure S12. Henry plots of all Tz-*df*-CTF materials as derived from CO_2, N_2, and CH_4 isotherms at T = 273 and 298K.

Section O. Productivity for CO_2/CH_4 Separation:

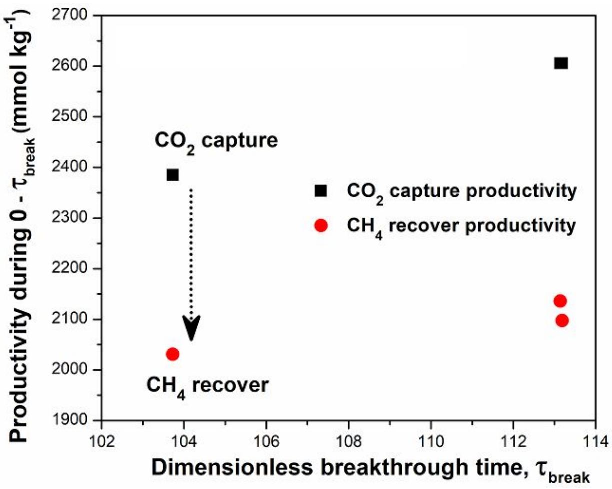

Figure S13. Comparison of CO_2 capture and CH_4 recovery productivity at 298 K.

Section P. Comparison Tables of Textural and Gas Uptake Properties:

Table S6. Comparison of surface area, CO_2 uptake (> 4 mmol g^{-1} at 273 K), Q_{st}, selectivity (CO_2/N_2) and H_2 uptake of Tz-*df*-CTF materials with notable POP based adsorbents at 1 bar.

POP-based Adsorbents	S_{BET} (m^2 g^{-1})	CO_2 Uptake [mmol g^{-1}]		Q_{st} [KJ mol^{-1}]	(CO_2/N_2) Selectivity at 298 K		H_2 Uptake [wt%]	Ref.
	77 K	273 K	298 K		Henry	IAST	77 K	

Tz-*df*-CTF600	2105	7.65	5.08	20.0	21.1	16.8	2.91	**Our work**
Tz-*df*-CTF500	1878	7.41	4.86	19.7	21.5	18.9	2.76	**Our work**
Tz-*df*-CTF400	1550	6.42	4.32	23.4	22.7	18.5	2.51	**Our work**
CQN-1e	1931	6.58	4.39	41.7	-	44.6	-	95
CQN-1g	1870	7.16	4.57	40.6	-	42.7	-	
NRPP-1	1579	6.10	2.22	28	21	21	-	94
NRPP-2	1028	7.06	3.71	29.1	24	36	-	
CPOP-1	2220	4.82	-	27	-	25[a]	2.80	98
PPF-1	1740	6.12	-	25.6	-	14.5[a]	2.75	89
PPF-2	1470	5.54	-	29.2	-	15.4[a]	2.28	
NPOF-1-NH_2	1535	5.84	3.77	32.1	-	25	-	S3
TPMTP	890	5.80	3.60	28.3	63[a]	61[a]	-	36
P-PCz	1647	5.57	2.97	30.9	32[a]	42[a]	-	90
ALP-1	1235	5.37	3.25	29.2	27	28	2.19	91
ALP-2	1065	4.80	2.46	27.9	27	26	1.74	
BILP-4	1135	5.34	3.59	28.7	32	-	2.30	S4
BILP-3	1306	5.11	3.30	28.6	31	-	2.10	
BILP-6	1261	4.80	2.75	28.4	39	-	2.20	
BILP-7	1122	4.39	2.77	27.8	34	-	1.80	
TBILP-2	1080	5.59	3.32	29.0	40	43	-	S5
TpPaCOF(MW)	724.6	5.10	2.00	34.1	-	32[a]	-	S6
COF-JLU-2	410	4.93	-	31	77	-	1.60	S7
N-PEINK	1836	4.86	-	31.3	97[a]	-	2.67	S8
Cz-POF-3	1927	4.77	-	27.8	23	20[a]	2.07	S9
Cz-POF-1	2065	4.59	-	25.3	19	17[a]	2.24	
Zn@AB-COF	1120	4.68	1.79	31.8	48	55	-	S10
Li@AB-COF	988	4.33	1.43	32.2	13	16	-	
MCTP-1	1452	4.64	2.70	40	15.4	-	-	S11
PP-N-25	1257	4.60	-	~35	-	-	-	S12
HEX-COF-1	1200	4.55	-	42	-	-	-	S13
APOP-3	1402	4.54	2.59	27.5	-	26.0	1.80	S14
APOP-1	1298	4.26	2.69	26.6	-	20.2	1.71	
SIOC-COF-5	707	4.50	-	-	-	-	1.66	S15
SNU-C1-sca	830	4.38	3.14	31.2	-	88	-	S16
CZ@PON	592	4.31	1.67	42.01	107	-	1.65	S17
BCzMB@PON	865	4.02	1.43	31.96	58	-	1.57	
Fe-POP-1	875	4.31	-	-	-	-	-	S18
HC-PCz-8	1688	4.30	3.50	20.4	17	-	-	S19

BILP-1	1172	4.27	2.98	26.5	36	-	1.90	S20
POF1B	917	4.23	2.16	-	-	-	1.25	S21
PPN-6-SO_3Li	1186	4.20	-	35.7	-	17[b]	-	35
STP-2	1990	4.14	-	-	-	-	1.93	S22
CPOP-9	2440	4.14	2.23	24.5	-	-	2.44	99
TSP-2	913	4.10	2.6	30.8	38	25	-	S23
TB-MOP	694	4.05	2.57	24.5	50.6	-	-	S24
BILP-10	787	4.02	~2.5	38.2	59	-	1.60	S25
PAN-2	1242	4.00	2.89	39.3	104[a]	50[a]	-	100

[a]measured at 273 K. [b]measured at 295 K.

Table S7. Comparison of structural parameters, CO_2 (> 4 mmol g^{-1} at 273 K) and H_2 uptakes, and CO_2/N_2 selectivity of Tz-*df*-CTF materials with other most representative related CTF-based adsorbents.

Only CTF-based adsorbents	**S_{BET} (m^2 g^{-1})**	**CO_2 Uptake [mmol g^{-1}]**		**Q_{st} [KJ mol^{-1}]**	**(CO_2/N_2) Selectivity at 298 K**		**H_2 Uptake [wt%]**	**Ref.**
	77 K	273 K	298 K		Henry	IAST	77 K	
Tz-*df*-CTF600	2105	7.65	5.08	20.0	21.1	16.8	2.91	**Our work**
Tz-*df*-CTF500	1878	7.41	4.86	19.7	21.5	18.9	2.76	**Our work**
Tz-*df*-CTF400	1550	6.42	4.32	23.4	22.7	18.5	2.51	**Our work**
HAT-CTF 450/600	1090	6.3	4.80[a]	27.1	126[a]	-	-	32
HAT-CTF-600	899	5.1	-	-	-	-	-	
HAT-CTF-450	756	4.4	-	-	-	-	-	
caCTF-1-700	2367	6.00	3.55	30.6	-	-	2.46	53
caCTF-2-700	1866	5.10	3.10	31.9	-	-	1.89	
F-DCBP-CTF-1	2437	5.98	3.82	33.1	31	-	1.77	55
F-DCBP-CTF-2	2036	5.23	3.16	-	22	-	-	
CTF-py^{HT}	3040	5.97	4.22	27.1	29	-	2.63	96
CTF-py	1239	5.08	3.79	35.1	45	-	1.63	
CTF-ph	1991	4.54	3.05	33.2	20	-	1.87	
CTF-ph^{HT}	2675	4.17	2.69	25.4	11	-	2.46	
bipy-CTF500	1548	5.34	3.07	34.2	61	42	1.63	56
bipy-CTF600	2479	5.58	2.95	34.4	37	24	2.10	
lut-CTF350	635	4.06	2.41	37.4	76	66	1.22	
lut-CTF400	968	4.55	2.72	37.5	63	53	1.36	
lut-CTF500	1680	5.04	2.58	38.2	27	27	1.60	
lut-CTF600	2815	4.99	2.52	33.3	26	23	2.00	
FCTF-1-600	1535	5.53	3.41	-	-	19	-	110

FCTF-1	662	4.67	3.21	35	-	31	-	
*p*CTF-1	2034	4.97	-	25.9	-		1.75	S26
TPC-1	1940	4.90	-	39	38^b		-	63
MM2	1360	4.77	-	32	23^b	44^b	1.74	68
PCTF-4	1404	4.65	2.86	~31	56^b	-	1.30	39
fl-CTF-350	1235	4.28	2.29	32.7	27	23	-	37
fl-CTF-400	2862	4.13	1.97	30.7	15	16	1.95	
CTF-0	2011	4.22	-	-	-	-	-	38
P6M	947	4.17	-	-	-	14.2^b		S27
PCTP-1	1200	4.91	3.24	44.5	46.1	-	-	S28
CTF-BI-4	1025	4.85	-	34.3–31.7	44.0^b	-	-	S29
CTF-BI-5	836	4.49	-		35.6^b	-	-	
CTF-BI-9	885	4.29	-		67.4^b	-	-	
CTF-BI-10	1099	4.45	-		31.3^b	-	-	
CTF-BI-11	1549	4.93	-		34.3^b	-	-	
MCTP-1	1452	4.64	2.69	40.0	15.4	-	-	S11
CTF-TPC	1668	4.25	-	32	20.0^b	30.0^b	1.75	S30

[a]measured at 297 K, [b]measured at 273 K.

Table S8. Comparison of surface area, CH_4 uptake (> 2 wt% at 273 K and 1 bar) and Q_{st} of other high-performing POP and CTF based adsorbents.

POP & CTF-based adsorbents	**S_{BET} ($m^2\ g^{-1}$)**	**CH_4 Uptake [wt%]**		**Q_{st} [KJ mol^{-1}]**	**Ref.**
	77K	**273 K**	**298 K**		
TPC-1	1940	6.2	-	-	63
Tz-*df*-CTF600	2105	4.41	2.20	24.0	**Our work**
Tz-*df*-CTF500	1878	4.13	2.08	22.5	**Our work**
Tz-*df*-CTF400	1550	3.64	1.73	27.4	**Our work**
PPOP-1	720	4.01	-	-	S31
PPOP-2	920	4.29	-	-	
PPOP-3	880	3.24	-	-	
COF-JLU2	415	3.80	1.80	20.5	S7
BDT-3	1010	2.9	-	-	S32
BILP-6-NH_2	1185	2.8	-	-	S33
TPMTP	890	2.7	-	-	36
PCTF-4	1404	2.7	-	-	39
BILP-6	1261	2.7	1.90	13.2	S34
BILP-3	1306	2.4	1.70	16.6	
ALP-1	1235	2.6	1.50	20.8	91
Cz-POF-3	1927	2.54	1.71^a	20.2	S9

Cz-POF-1	2065	2.29	1.56[a]	19	
BILP-4	1135	2.53	1.80	13.0	S4
PPF-1	1740	2.43	-	15.1	89
PPF-2	1470	2.31	-	15.9	
BILP-12	1497	2.4	1.50	18.6	S35
TNP-4	1348	2.38	1.42	20	S36
MM2	1360	2.34	1.51[b]	-	68
MM1	1800	2.06	1.34[b]	-	
HEX-COF-1	1200	2.30	1.20	27	S13
APOP-3	1402	2.20	1.20	19.5	S14
APOP-1	1298	2.13	1.25	18	
CTF-TPC	1668	2.14	-	-	S32
PAF-60	1094	2.0	1.50	24.1	S37
JUC-Z8	4743	2.0	-	-	S38

Table S9. Comparison of porosity and gas sorption properties of Tz-*df*-CTFs with the current benchmark porous organic polymers.

POP-based Adsorbents	**S_{BET} (m^2 g^{-1})**	**CO_2 Uptake [mmol g^{-1}]**		**CH_4 Uptake [wt%]**	**H_2 Uptake [wt%]**	**Ref.**
	77 K	**273 K**	**298 K**	**273 K**	**77 K**	
Tz-*df*-CTF400	1550	6.42 (2.32)	4.32 (1.33)	3.63	2.51	**Our work**
Tz-*df*-CTF500	1878	7.41(2.34)	4.86 (1.35)	4.12	2.76	**Our work**
Tz-*df*-CTF600	2106	7.65 (2.39)	5.08 (1.36)	4.41	2.91	**Our work**
CQN-1g	1870	7.16	4.57	-	-	95
NRPP-2	1028	7.06	3.71	-	-	94
HAT-CTFs	1090	6.30 (3.0)	4.8 (2.0)*	-	-	32
PPF-1	1740	6.12	-	2.43	2.75	89
CTF-py^{HT}	3040	5.97	4.22	-	2.63	96
CPOP-1	2220	4.82	-	-	2.80	98
TPC-1	1940	4.90	-	6.20	2.00	63

*measured at 297 K; values in parenthesis in mmol g^{-1} at 0.15 bar

Section Q. High Pressure H_2 Adsorption Isotherms:

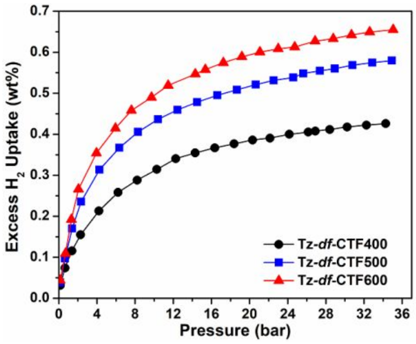

Figure S14. Excess H_2 isotherms of Tz-*df*-CTFs at 298 K.

High-pressure (up to 35 bar) H_2 adsorption measurements were also performed at 298 K and the resulting isotherms for Tz-*df*-CTFs are presented in **Figure S14** with uptake capacity up to 0.65 wt% (at 35 bar, 298 K) for Tz-*df*-CTF600, which is higher than those of many best-known porous materials under similar measurement conditions.[58,S39-S40]

Section R. Supporting References:

S1:	Tobe, Y.; Nakagawa, N.; Kishi, J.; Sonoda, M.; Naemura, K.; Wakabayashi, T.; Shida, T.; Achiba, Y. Polyyne Cyclization to form Carbon Cages: [16.16.16] (1,3,5) Cyclophanetetracosayne Derivatives $C_{60}H_6$ and $C_{60}Cl_6$ as Precursors to C_{60} Fullerene. *Tetrahedron* **2001**, *57*, 3629-3636.
S2:	Farha, O. K.; Yazaydın, A. Ö.; Eryazici, I.; Malliakas, C. D.; Hauser, B. G.; Kanatzidis, M. G.; Nguyen, S. T.; Snurr, R. Q.; Hupp, J. T. *De Novo* Synthesis of a Metal–Organic Framework Material Featuring Ultrahigh Surface Area and Gas Storage Capacities. *Nature Chemistry* **2010,** *2*, 944-948.
S3:	Islamoglu, T.; Kim, T.; Kahveci. Z.; El-Kadri, O.M.; El-Kaderi, H. M. Systematic Postsynthetic Modification of Nanoporous Organic Frameworks for Enhanced CO_2 Capture from Flue Gas and Landfill Gas. *J. Phys. Chem. C* **2016**, *120*, 2592-2599.
S4:	Rabbani, M. G.; El-Kaderi, H. M. Synthesis and Characterization of Porous Benzimidazole-Linked Polymers and Their Performance in Small Gas Storage and Selective Uptake. *Chem. Mater.* **2012**, *24,* 1511-1517.
S5:	Sekizkardes, A. K.; Altarawneh, S.; Kahveci, Z.; İslamoğlu, T.; El-Kaderi, H. M. Highly Selective CO_2 Capture by Triazine-Based Benzimidazole-Linked Polymers. *Macromolecules* **2014**, *47*, 8328-8334.
S6:	Wei, H.; Chai, S.; Hu, N.; Yang, Z.; Wei, L.; Wang, L. The Microwave-Assisted Solvothermal Synthesis of a Crystalline Two-Dimensional Covalent Organic Framework with High CO_2 Capacity. *Chem. Commun.* **2015**, *51*, 12178-12181.
S7:	Li, Z.; Zhi, Y.; Feng, X.; Ding, X.; Zou, Y.; Liu, X.; Mu, Y. An Azine-Linked Covalent Organic Framework: Synthesis, Characterization and Efficient Gas Storage. *Chem. Eur. J.* **2015**, *21*, 12079-12084.
S8:	Chang, G.; Yang, L.; Yang, J.; Huang, Y.; Cao, K.; Ma, J.; Wang, D. A Nitrogen-Rich, Azaindole-Based Microporous Organic Network: Synergistic Effect of Local Dipole-π and Dipole-Quadrupole Interactions on Carbon Dioxide Uptake. *Polym. Chem.* **2016**, *7*, 5768-5772.

S9:	Zhang, X.; Lu, J.; Zhang, J. Porosity Enhancement of Carbazolic Porous Organic Frameworks Using Dendritic Building Blocks for Gas Storage and Separation. *Chem. Mater.* **2014**, *26*, 4023-4029.
S10:	Stegbauer, L.; Hahn, M. W.; Jentys, A.; Savasci, G.; Ochsenfeld, C.; Lercher, J. A.; Lotsch, B. V. Tunable Water and CO_2 Sorption Properties in Isostructural Azine-Based Covalent Organic Frameworks through Polarity Engineering. *Chem. Mater.* **2015**, *27*, 7874-7881.
S11:	Puthiaraj, P.; Cho, S. –M.; Lee, Y. –R.; Ahn, W. -S. Microporous Covalent Triazine Polymers: Efficient Friedel-Crafts Synthesis and Adsorption/Storage of CO_2 and CH_4. *J. Mater. Chem. A* **2015**, *3*, 6792-6797.
S12:	Yang, Y.; Zhang, Q.; Zhang, S.; Li, S. Synthesis and Characterization of Triphenylamine-Containing Microporous Organic Copolymers for Carbon Dioxide Uptake. *Polymer,* **2013**, *54*, 5698-5702.
S13:	Alahakoon, S. B.; Thompson, C. M.; Nguyen, A. X.; Occhialini, G.; McCandless, G. T.; Smaldone, R. A. An Azine-Linked Hexaphenylbenzene Based Covalent Organic Framework. *Chem. Commun.* **2016**, *52*, 2843-2845.
S14:	Song, W. -C.; Xu, X. -K.; Chen, Q.; Zhuang, Z. -Z.; Bu, X. -H. Nitrogen-Rich Diaminotriazine-Based Porous Organic Polymers for Small Gas Storage and Selective Uptake. *Polym. Chem.* **2013**, *4*, 4690-4696.
S15:	Tian, Y.; Xu, S. -Q.; Qian, C.; Pang, Z. -F.; Jiang, G. -F.; Zhao, X. Two-Dimensional Dual-Pore Covalent Organic Frameworks Obtained From the Combination of Two D_{2h} Symmetrical Building Blocks. *Chem. Commun.* **2016**, *52*, 11704-11707.
S16:	Xie, L. -H.; Suh. M. P. High CO_2-Capture Ability of a Porous Organic Polymer Bifunctionalized with Carboxy and Triazole Groups. *Chem. Eur. J.* **2013**, *19*, 11590-11597.
S17:	Mondal, S.; Kundu, S. K.; Bhaumik, A. A Facile Approach for the Synthesis of Hydroxyl-Rich Microporous Organic Networks for Efficient CO_2 Capture and H_2 Storage. *Chem. Commun.* **2017**, *53*, 2752-2755.
S18:	Modak, A.; Nandi, M.; Mondal, J.; Bhaumik, A. Porphyrin Based Porous Organic Polymers: Novel Synthetic Strategy and Exceptionally High CO_2 Adsorption Capacity. *Chem. Commun.* **2012**, *48*, 248-250.
S19:	Zhu, X.; Ding, S.; Abney, C. W.; Browning, K. L.; Sacci, R. L.; Veith, G. M.; Tian, C.; Dai, S. Superacid-Promoted Synthesis of Highly Porous Hypercrosslinked Polycarbazoles for Efficient CO_2 Capture. *Chem. Commun.* **2017**, *53*, 7645-7648.
S20:	Rabbani, M. G.; El-Kaderi, H. M. Template-Free Synthesis of a Highly Porous Benzimidazole-Linked Polymer for CO_2 Capture and H_2 Storage. *Chem. Mater.* **2011**, *23*, 1650-1653.
S21:	Katsoulidis, A. P.; Kanatzidis, M. G. Phloroglucinol Based Microporous Polymeric Organic Frameworks with -OH Functional Groups and High CO_2 Capture Capacity. *Chem. Mater.* **2011**, *23*, 1818-1824.
S22:	Zhang, C.; Ying Liu, Y.; Li, B.; Tan, B.; Chen, C. –F.; Xu, H. –B.; Yang, X. –L. Triptycene-Based Microporous Polymers: Synthesis and Their Gas Storage Properties. *ACS Macro Lett.* **2012**, *1*, 190-193.

S23:	Zhu, X.; Mahurin, S. M.; An, S. –H.; Do-Thanh, C. –L.; Tian, C.; Li, Y.; Gill, L. W.; Hagaman, E. W.; Bian, Z.; Zhou, J. –H.; Hu, J.; Liu, H.; Dai, S. Efficient CO_2 Capture by a Task-Specific Porous Organic Polymer Bifunctionalized with Carbazole and Triazine Groups. *Chem. Commun.* **2014**, *50*, 7933-7936.
S24:	Zhu, X.; Do-Thanh, C. -L.; Murdock, C. R.; Nelson, K. M.; Tian, C.; Brown, S.; Mahurin, S. M.; Jenkins, D. M.; Hu, J.; Zhao, B.; Liu, H.; Dai, S. Efficient CO_2 Capture by a 3D Porous Polymer Derived from Tröger's Base. *ACS Macro Lett.* **2013**, *2*, 660-663.
S25:	Rabbani, M. G.; Sekizkardes, A. K.; El-Kadri, O. M.; Kaafarani, B. R.; El-Kaderi, H. M. Pyrene-Directed Growth of Nanoporous Benzimidazole-Linked Nanofibers and their Application to Selective CO_2 Capture and Separation. *J. Mater. Chem.* **2012**, *22*, 25409-25417.
S26:	Yu, S. -Y.; Mahmood, J.; Noh, H. -J.; Seo, J. -M.; Jung, S. -M.; Shin, S. -H.; Im, Y. -K.; Jeon, I. -Y.; Baek, J. -B. Direct Synthesis of a Covalent Triazine-Based Framework from Aromatic Amides. *Angew. Chem. Int. Ed.* **2018**, *57*, 8438-8442.
S27	Ren, S.; Bojdys, M. J.; Dawson, R.; Laybourn, A.; Khimyak, Y. Z.; Adams, D. J.; Cooper, A. I. Porous, Fluorescent, Covalent Triazine-Based Frameworks Via Room-Temperature and Microwave-Assisted Synthesis. *Adv. Mater.* **2012**, *24*, 2357-2361.
S28	Puthiaraj, P.; Kim, S. -S.; Ahn, W. -S. Covalent Triazine Polymers Using a Cyanuric Chloride Precursor Via Friedel–Crafts reaction for CO_2 adsorption/separation. *Chem. Eng. J.* **2016**, *283*, 184-192.
S29	Tao, L.; Niub, F.; Wanga, C.; Liuc, J.; Wanga, T.; Wang, Q. Benzimidazole Functionalized Covalent Triazine Frameworks for CO_2 Capture. *J. Mater. Chem. A* **2016**, *4*, 11812-11820.
S30	Dey, S.; Bhunia, A.; Esquivel, D.; Janiak, C. Covalent Triazine-Based Frameworks (CTFs) from Triptycene and Fluorene Motifs for CO_2 Adsorption. *J. Mater. Chem. A* **2016**, *4*, 6259-6263.
S31	Wang, T.; Zhao, Y. -C.; Zhang, L. -M.; Cui, Y.; Zhang, C. -S.; Han, B. -H. Novel Approach to Hydroxy-Group-Containing Porous Organic Polymers from Bisphenol A. *Beilstein J. Org. Chem.* **2017,** *13,* 2131-2137.
S32	Bandyopadhyay, S.; Anil, A. G.; James, A.; Patra, A. Multifunctional Porous Organic Polymers: Tuning of Porosity, CO_2, and H_2 Storage and Visible-Light-Driven Photocatalysis. *ACS Appl. Mater. Interfaces* **2016**, *8,* 27669-27678.
S33	Islamoglu, T.; Behera, S.; Kahveci, Z.; Tessema, T. –D.; Jena, P.; El-Kaderi, H. M. Enhanced Carbon Dioxide Capture from Landfill Gas Using Bifunctionalized Benzimidazole-Linked Polymers. *ACS Appl. Mater. Interfaces* **2016**, *8,* 14648-14655.
S34	Rabbani, M. G.; Reich, T. E.; Kassab, R. M.; Jackson, K. T.; El-Kaderi, H. M. High CO_2 Uptake and Selectivity by Triptycene-Derived Benzimidazole-Linked Polymers. *Chem. Commun.* **2012**, *48*, 1141-1143.
S35	Sekizkardes, A. K.; İslamoğlu, A.; Kahveci, Z.; El-Kaderi, H. M. Application of Pyrene-Derived Benzimidazole-Linked Polymers to CO_2 Separation under Pressure and Vacuum Swing Adsorption Settings. *J. Mater. Chem. A* **2014**, *2*, 12492-12500.

S36	Mondal, S.; Das, N. Triptycene Based 1,2,3-Triazole Linked Network Polymers (TNPs): Small Gas Storage and Selective CO_2 Capture. *J. Mater. Chem. A* **2015**, *3*, 23577-23586.
S37	Yuan, Y.; Cui, P.; Tian, Y.; Zou, X.; Zhou, Y.; Sun, F.; Zhu, G. Coupling Fullerene into Porous Aromatic Frameworks for Gas Selective Sorption. *Chem. Sci.* **2016**, *7*, 3751-3756.
S38	Pei, C.; Ben, T.; Li, Y.; Qiu, S. Synthesis of Copolymerized Porous Organic Frameworks with High Gas Storage Capabilities at Both High and Low Pressures. *Chem. Commun.* **2014**, *50*, 6134-6136.
S39	Panella, B.; Hirscher, M.; Pütter, H.; Müller, U. Hydrogen Adsorption in Metal–Organic Frameworks: Cu-MOFs and Zn-MOFs Compared. *Adv. Funct. Mater.* **2006**, *16*, 520-524.
S40	Stadie, N. P.; Vajo, J. J.; Cumberland, R. W.; Wilson, A. A.; Ahn, C. C.; Fultz, B. Zeolite-templated carbon materials for high-pressure hydrogen storage. *Langmuir* **2012**, *28*, 10057-10063.